Journal of Computational Applied Mechanics 2023, 54(4): 482-500

DOI: 10.22059/JCAMECH.2023.366194.885

RESEARCH PAPER

Bending Response of a Rotating Viscoelastic Functionally Graded Porous Disk with Variable Thickness

Rania M. Tantawy [a,*], Ashraf M. Zenkour [b,c,1]

[a] *Department of Mathematics, Faculty of Science, Damietta University, P.O. Box 34517, Egypt*
[b] *Department of Mathematics, Faculty of Science, King Abdul-Aziz University, P.O. Box 80203, Jeddah 21589, Saudi Arabia*
[c] *Department of Mathematics, Faculty of Science, Kafrelsheikh University, Kafrelsheikh 33516, Egypt*

Abstract

The analysis of the bending behavior of rotating porous disks with exponential thickness variation consisting of viscoelastic functionally graded material is illustrated. The study of bending in the porous disk was done using the first-order shear deformation theory. The porous disk is under the effect of a combination of mechanical stresses and thermal distribution. All material factors for the porous disk change across the thickness as a power law of radius. To solve the mathematical structure by using the semi-analytical technique for displacements in the porous disk, and then to treat the structure model with viscoelastic material by the correspondence principle and Illyushin's approximation manner. Numerical outcomes including the effect of porosity parameter, inhomogeneity factor, and relaxation time are presented with three different sets of boundary conditions for the solid and hollow disks. A comparison between porous and perfect disk with numerous values of porosity parameters and different inhomogeneity factors have been shown to emphasize the importance of complex mathematical structure in modern engineering mechanical designs.

Keywords: Inhomogeneity; porosity; semi-analytical technique; Illyushin's method; viscoelasticity.

1. Introduction

The development of the industry day after day increases the need to develop composite materials and enhance their properties. It was therefore necessary to develop new materials with graded properties to meet the requirements of engineering designs and applications. Most modern industrial applications in the automotive, aerospace, missiles, and mobile phones require a material that changes gradually in certain directions. Therefore, functionally graded materials (FGM) were designed for the first time in the Japanese Space Shuttle project in 1983. With the development of industry, the porosity feature appeared in functionally graded materials, which recently have been widely used in the fields of bioengineering, electronic equipment, and other fields.

Chen et al. [1] studied the irregular porosity distribution and vibration properties of FG porous beams. Tantawy and Zenkour [2] investigated the influence of porosity on FG piezoelectric hollow spheres with electrical and mechanical loads in a hygrothermal environment. Saadatfar et al. [3] considered a mathematical model of a porous disc to study its free vibration. Many studies have been presented to study the porosity property in gradient materials, for example [4-10].

Functionally graded viscoelastic materials can be counted as one of the newest materials of the gradient family of materials. Due to the originality of the gradient viscoelastic materials, they have attracted many researchers to study their properties. Norouzi et al. [11] examined the analysis of FG viscoelastic cylindrical panels. Allam et al. [12] discussed numerical and analytical solutions for FG viscoelastic annular and solid disks by successive approximations technique. Dave et al. [13] offered an FG viscoelastic model to examine the asphalt responses affected by mechanical load and thermal distribution. Kim et al. [14] investigated the semi-analytical solution for a nonlinear FG viscoelastic plate for dynamic and vibration response. Other studies and research have appeared in [15-23].

Many researchers began to explore the bending and vibration of porous panels made from a gradient material. The distribution of the porous has a significant effect on the plate's dynamics. From this research, Coskun et al. [24] use the third-order plate theory to study the vibration and buckling of FG porous plates. The same theory was also used to examine the effectiveness of porosity and inhomogeneity on FG porous sandwiches by Daikh and Zenkour [25]. The theory is deduced by Zenkour [26, 27] to solve the problems of the 3D FG porous plates problems that are single-layer, piezoelectric, and sandwich plates. Additional research and studies have appeared in [28-32].

[1] Corresponding author.
E-mail address: zenkour@kau.edu.sa, zenkour@sci.kfs.edu.eg

Theoretical and numerical studies of the thermomechanical effect on the viscoelastic FG rotating solid and hollow disk with exponentially variable thickness are presented. Using the first-order shear deformation theory we can study the bending acting on the viscoelastic porous disk. Thermal and mechanical coefficients are pretended to be graded along the thickness as a power law in radius by taking into consideration the inhomogeneity factor and porosity parameter. As a first step, using the semi-analytical method, the governing differential equation is solved. In the second step, the correspondence principle with Illyushin's approximation technique is exploited to solve the viscoelastic porous disk. The numerical outcomes are gained for three different sets of solid and hollow disks. The outcomes numerical results are compared and the influence of different parameters affecting the disk is discussed.

2. Nomenclature

a	internal radii of the disk [m]
b	external radii of the disk [m]
E	Young's modulus [GPa]
ν	Poisson's ratio
$H(t)$	Heaviside unit step function
h_0	thickness of the center of disk [m]
K_T	coefficient of heat conductivity [W/K m]
n	inhomogeneity factor
ω	angular velocity
$s^{(k)}$	radial width of the k^{th} subsection [m]
q_z	perpendicular pressure [Pa]
T_0	reference temperature [K]
α	thermal expansion factor [K^{-1}]
β	porosity parameter
N_r, N_θ	non-dimensional forces per unit length
M_r, M_θ	non-dimensional moments per unit length
$h(r)$	thickness changing [m]
Q_r	non-dimensional transeverse shear resultant
l, k	profile characteristic
$r^{(k)}$	the mean radius of the k^{th} subsection [m]
T_1	temperature on external radii [K]
ρ	density [$\mathrm{kg\,m}^{-3}$]
$p^{(a)}$	properties of internal surface
$p^{(b)}$	internal radii of the disk [m]

3. Geometric shape of the porous graded disk

Consider graded viscoelastic porous disk with variable thickness $h(r)$, internal radii a, external radii b. The disk orbits about the z-axis with angular speed ω. The disk is exposed to transverse loading $q_z(r)$, thermal distribution $T(r)$ and mechanical loading. According to the geometric disk profile, the cylindrical coordinate (r, θ, z) are used. The physical material coefficients are graded from PZT-4 to Cadmium Selenide as presented in Table 1.

Table 1. Thermal and mechanical coefficients of porous disk materials.

PZT-4 (Ootao and Tanigawa [33])	Cadmium selenide (Arani *et al.*[34])
$E^{(a)} = 84(\mathrm{GPa})$	$E^{(b)} = 50(\mathrm{GPa})$
$\nu^{(a)} = 0.31$	$\nu^{(b)} = 0.35$
$K_{\mathrm{T}}^{(a)} = 110\ (\mathrm{WK^{-1}m^{-1}})$	$K_{\mathrm{T}}^{(b)} = 4\ (\mathrm{WK^{-1}m^{-1}})$
$\alpha_r^{(a)} = 2 \times 10^{-5}\ (\mathrm{K^{-1}})$	$\alpha_r^{(b)} = 2.458 \times 10^{-6}\ (\mathrm{K^{-1}})$
$\rho^{(a)} = 7500(\mathrm{kg\,m^{-3}})$	$\rho^{(b)} = 5684(\mathrm{kg\,m^{-3}})$

3.1 *Thickness modulation description*

The thickness variation of the exponentially viscoelastic porous disk has a mathematical formulation [35, 36].

$$h(r) = h_0 \mathrm{e}^{-l\left(\frac{r}{b}\right)^k}, \tag{1}$$

where h_0 is the thickness of the disk center and l, k are geometric coefficients that define the thickness of the edge and shape of the disk profiles

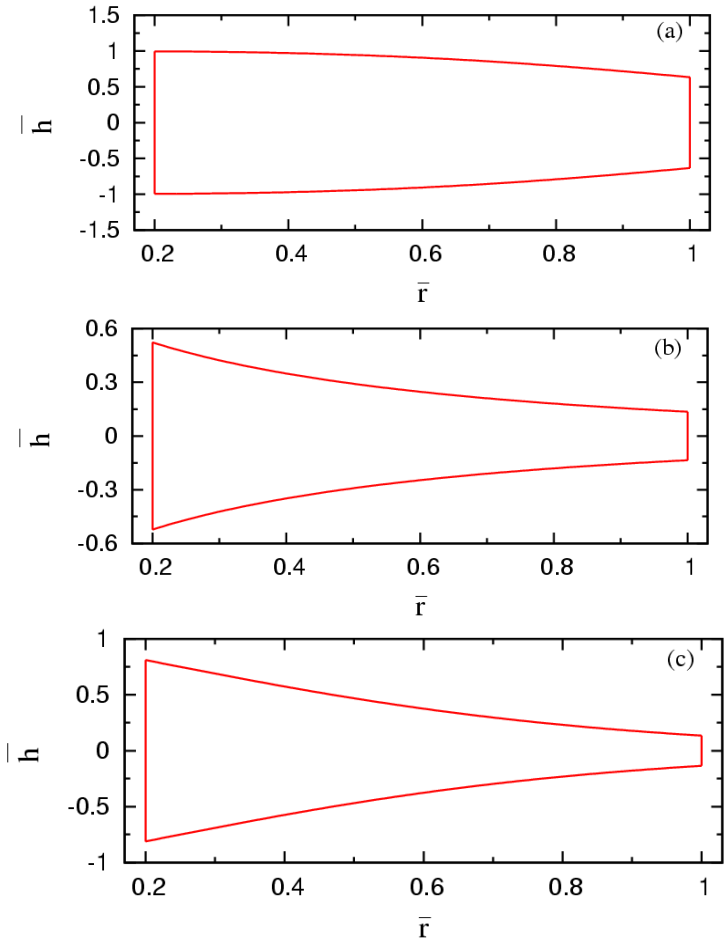

Fig. 1. Exponential viscoelastic porous disk thickness description
(a) $l = 0.4568,\ k = 3$, **(b)** $l = 2,\ k = 0.7$, **and (c)** $l = 2,\ k = 1.4$.

3.2 *Porosity gradient of exponential porous disks*

In this research, we postulate that the thermal and mechanical coefficients of the disk difference in the direction of the radius by a power function on the mathematical formula p(r) as

$$p(r) = \left(p^{(b)} - p^{(a)}\right)\left(\frac{r-a}{b-a}\right)^{n} + p^{(a)} - \frac{\beta}{2}\left(p^{(b)} + p^{(a)}\right), \tag{2}$$

where $p^{(a)}$ and $p^{(b)}$ are internal and external properties surfaces, $n \geq 0$ is the inhomogeneity factor and $0 \leq \beta \leq 1$ is the porosity parameter when $\beta = 0$ means non-porous (perfect) disk.

3.3 *Thermal equation*

The thermal equation for gradient porous disk is given by the equation [37]

$$\frac{1}{rh(r)}\frac{\mathrm{d}}{\mathrm{d}r}\left(r\,k_T\,h(r)\frac{\mathrm{d}T(r)}{\mathrm{d}r}\right) = 0, \tag{3}$$

where k_T is the coefficient of heat conductivity and satisfies the gradient relationship (2).
Thermal boundary conditions for the gradient porous disk

$$T(r)|_{r=a} = T_0, \quad T(r)|_{r=b} = T_1, \tag{4}$$

where T_0 is reference temperature and T_1 is the temperature on external radii.

3.4 *Basic equilibrium differential equations*

The governing equations for a rotating graduated porous disk of changing thickness using first-order shear deformation theory, which imposes that the transverse shear component remains not equal to zero, and its value is specified and constant throughout the disk thickness, and displacement components are imposed in the form

$$u_r(r,z) = u_0 + z\psi, \quad u_\theta = 0, \quad u_z(r,z) = w. \tag{5}$$

The strain components are given through the mathematical relationships [38]

$$\left.\begin{aligned} \varepsilon_r = \frac{\partial u_r}{\partial r} = \frac{\mathrm{d}u_0}{\mathrm{d}r} + z\frac{\mathrm{d}\psi}{\mathrm{d}r} \\ \varepsilon_\theta = \frac{u_r}{r} = \frac{u_0}{r} + z\frac{\psi}{r} \\ \gamma_{rz} = 2\varepsilon_{rz} = \frac{\partial u_r}{\partial z} + \frac{\partial u_z}{\partial r} = \psi + \frac{\mathrm{d}w}{\mathrm{d}r} \\ \gamma_{r\theta} = 2\varepsilon_{r\theta} = 0, \quad \gamma_{\theta z} = 2\varepsilon_{\theta z} = 0, \quad \varepsilon_z = \frac{\partial u_z}{\partial z} = 0 \end{aligned}\right\} \tag{6}$$

The constitutive equations of the porous disk are defined as

$$\left.\begin{aligned} \sigma_r = \frac{E}{1-\nu^2}\varepsilon_r + \frac{E\nu}{1-\nu^2}\varepsilon_\theta - \frac{E}{1-\nu}\alpha T \\ \sigma_\theta = \frac{E}{1-\nu^2}\varepsilon_\theta + \frac{E\nu}{1-\nu^2}\varepsilon_r - \frac{E}{1-\nu}\alpha T \\ \sigma_{rz} = \frac{E}{2(1+\nu)}\gamma_{rz} \end{aligned}\right\} \tag{7}$$

To study the equilibrium in the porous disk, if E_ε is the overall strain energy of porous disk and E_w is overall external work on a porous disk. From it, the total energy E can be deduced in the form $E \equiv E_\varepsilon - E_w$, where

$$\left.\begin{aligned} E_\varepsilon = \int_V \sigma_{ij}\varepsilon_{ij}\mathrm{d}V = \int_a^b \int_{-\frac{h(r)}{2}}^{\frac{h(r)}{2}} 2\pi(\sigma_r\varepsilon_r + \sigma_\theta\varepsilon_\theta + \sigma_{rz}\gamma_{rz})r\mathrm{d}z\mathrm{d}r \\ E_w = -\int_a^b \int_{-\frac{h(r)}{2}}^{\frac{h(r)}{2}} 2\pi\rho(r)r^2\omega^2 u_r\mathrm{d}z\mathrm{d}r - \int_a^b 2\pi r q_z(r)u_z\mathrm{d}r \end{aligned}\right\} \tag{8}$$

here $q_z(r)$ is the perpendicular pressure on a porous disk surface. From the principle of lower total energy $\delta E = 0$

$$\int_a^b \left\{\left(N_\theta - \frac{\mathrm{d}(rN_r)}{\mathrm{d}r} - \rho_1 r^2\omega^2\right)\delta u_0 + \left(M_\theta + rQ_r - \frac{\mathrm{d}(rM_r)}{\mathrm{d}r}\right)\delta\psi - \left(\frac{\mathrm{d}(rQ_r)}{\mathrm{d}r} + rq_z\right)\delta w\right\}\mathrm{d}r = 0, \tag{9}$$

where N_r, N_θ, M_r, M_θ, Q_r and ρ_1 are functions of r as

$$\left.\begin{aligned} (N_r, N_\theta, Q_r) = \int_{-\frac{h(r)}{2}}^{\frac{h(r)}{2}} (\sigma_r, \sigma_\theta, \sigma_{rz})\mathrm{d}z \\ (M_r, M_\theta) = \int_{-\frac{h(r)}{2}}^{\frac{h(r)}{2}} (\sigma_r, \sigma_\theta)\mathrm{z}dz \\ \rho_1 = \int_{-\frac{h(r)}{2}}^{\frac{h(r)}{2}} \rho(r)\mathrm{d}z = h(r)\rho(r) \end{aligned}\right\} \tag{10}$$

where N_r, N_θ and M_r, M_θ are forces and moments, respectively, for unit length; Q_r is transverse shear for the porous disk. From Eq. (9) yields

$$\left.\begin{aligned} -\frac{d(rN_r)}{dr} + N_\theta - \rho_1 r^2\omega^2 = 0 \\ -\frac{d(rM_r)}{dr} + M_\theta + rQ_r = 0 \\ \frac{d(rQ_r)}{dr} + rq_z = 0 \end{aligned}\right\} \tag{11}$$

Substituting from Eqs. (7) into Eqs. (10) we get

$$\left.\begin{aligned} N_r = \frac{hE}{(1-\nu^2)}\left[\frac{du_0}{dr} + \nu\frac{u_0}{r} - (1+\nu)\alpha T\right] \\ N_\theta = \frac{hE}{(1-\nu^2)}\left[\nu\frac{du_0}{dr} + \frac{u_0}{r} - (1+\nu)\alpha T\right] \\ M_r = \frac{h^3E}{12(1-\nu^2)}\left[\frac{d\psi}{dr} + \nu\frac{\psi}{r}\right] \\ M_\theta = \frac{h^3E}{12(1-\nu^2)}\left[\nu\frac{d\psi}{dr} + \frac{\psi}{r}\right] \\ Q_r = \frac{hE}{2(1+\nu)}k_s\left[\psi + \frac{dw}{dr}\right] \end{aligned}\right\} \tag{12}$$

here k_s is a shear-correction parameter. Considering that E, ν, ρ, and α are functions of the radius according to the gradient relation (2). By substituting Eqs. (12) into Eqs. (11), a system of differential equations is produced. By solving them, we can obtain the displacement components

$$\begin{aligned} rhE\frac{\mathrm{d}^2u_0}{\mathrm{d}r^2} + \left(\frac{\mathrm{d}(rhE)}{\mathrm{d}r} + \frac{2rhE\nu}{(1-\nu^2)}\frac{\mathrm{d}\nu}{\mathrm{d}r}\right)\frac{du_0}{dr} + \left(\frac{\nu}{r}\frac{\mathrm{d}(rhE)}{\mathrm{d}r} + rhE\left(1 + \frac{2\nu^2}{r(1-\nu^2)}\frac{d\nu}{dr} - \frac{hE(1+\nu)}{r}\right)\right)u_0 \\ +\rho r^2\omega^2 h(1-\nu^2) - r(1+\nu)\frac{\mathrm{d}(hE\alpha T)}{\mathrm{d}r} = 0, \end{aligned} \tag{13}$$

$$rhE\frac{\mathrm{d}^2\psi}{\mathrm{d}r^2}+\left(\frac{1}{h^2}\frac{\mathrm{d}(rh^3E)}{\mathrm{d}r}+\frac{2rhE\nu}{(1-\nu^2)}\frac{\mathrm{d}\nu}{\mathrm{d}r}\right)\frac{\mathrm{d}\psi}{\mathrm{d}r}+\frac{6(\nu-1)Erk_s}{h}\frac{\mathrm{d}w}{\mathrm{d}r}$$
$$+\left(\frac{\nu}{rh^2}\frac{\mathrm{d}(rh^3E)}{\mathrm{d}r}+hE\left(1+\frac{2\nu^2}{1-\nu^2}\right)\frac{\mathrm{d}\nu}{\mathrm{d}r}-\frac{hE(\nu+1)}{r}+\frac{6(\nu-1)Erk_s}{h}\right)\psi=0,$$
$$rhE\left(\frac{\mathrm{d}^2w}{\mathrm{d}r^2}+\frac{\mathrm{d}\psi}{\mathrm{d}r}\right)+\left(\frac{\mathrm{d}(rhE)}{\mathrm{d}r}-\frac{rhE}{1+\nu}\frac{\mathrm{d}\nu}{\mathrm{d}r}\right)\left(\frac{\mathrm{d}w}{\mathrm{d}r}+\psi\right)+\frac{2rq_z(1+\upsilon)}{k_s}=0.$$

To explain the influence of inhomogeneity and porosity on bending porous disk by changing thickness, we impose three different classes of boundary conditions on the porous disk [39]

Status 1: Circular solid porous disk

$$\left.\begin{array}{ll}\text{at } r=0 & u_0=0,\quad \psi=0,\quad Q_r=0,\\ \text{at } r=b & w=0,\quad N_r=0,\quad M_r=0.\end{array}\right\} \tag{14}$$

Status 2: Mounted free hollow porous disk

$$\left.\begin{array}{ll}\text{at } r=a & u_0=0,\quad \psi=0,\quad w=0,\\ \text{at } r=b & Q_r=0,\quad N_r=0,\quad M_r=0.\end{array}\right\} \tag{15}$$

Status 3: Mounted hollow supported cased porous disk

$$\left.\begin{array}{ll}at\ r=a & u_0=0,\quad \psi=0,\quad w=0,\\ at\ r=b & w=0,\quad N_r=0,\quad M_r=0.\end{array}\right\} \tag{16}$$

4. Elastic solution for gradient porous disk

Obtaining the analytical mathematical solution for the thermal differential equation (3) and the system of differential equations (13) with the aid of the thickness equation (1) and the equation for the gradient of properties and porosity (2) is not easy, but rather very difficult. This is because the displacements in the system of differential equations (13) as well as the thermal equation (3) are considered functions of the radius r. Using the semi-analytical method to solve the system of equations, where the radial range from $r=a$ to $r=b$ is divided into several subsections, each of which has a thickness $s^{(k)}$ and an average radius of each subsection, $r^{(k)}$, as shown in Fig. 2. By referring to thermal equation (3) and the system of differential equations (13) and calculating the coefficients at $r=r^{(k)}$, the system of equations turns to:

$$\left.\begin{array}{c}\left(c_1^{(k)}D^2+c_2^{(k)}D+c_3^{(k)}\right)u_0^{(k)}+c_4^{(k)}=0\\ \left(c_1^{(k)}D^2+c_5^{(k)}D+c_6^{(k)}+c_7^{(k)}\right)\psi^{(k)}+c_7^{(k)}Dw^{(k)}=0\\ \left(c_1^{(k)}D^2+c_8^{(k)}D\right)w^{(k)}+\left(c_1^{(k)}D+c_8^{(k)}\right)\psi^{(k)}+c_9^{(k)}=0\end{array}\right\} \tag{17}$$

where $D=\frac{\mathrm{d}}{\mathrm{d}r}$,

$$c_1^{(k)}=r^{(k)}h\left(r^{(k)}\right)E\left(r^{(k)}\right),$$
$$c_2^{(k)}=\frac{\mathrm{d}c_1}{\mathrm{d}r}\Big|_{r=r^{(k)}}+\frac{2\nu\left(r^{(k)}\right)c_1^{(k)}}{1-\left(\nu\left(r^{(k)}\right)\right)^2}\frac{\mathrm{d}\nu(r)}{\mathrm{d}r}\Big|_{r=r^{(k)}},$$
$$c_3^{(k)}=\frac{\nu\left(r^{(k)}\right)}{r^{(k)}}\frac{\mathrm{d}c_1}{\mathrm{d}r}\Big|_{r=r^{(k)}}+c_1^{(k)}\left(1+\frac{2\left(\nu\left(r^{(k)}\right)\right)^2}{r^{(k)}\left(1-\left(\nu\left(r^{(k)}\right)\right)^2\right)}\right)\frac{\mathrm{d}\nu(r)}{\mathrm{d}r}\Big|_{r=r^{(k)}}-\frac{h\left(r^{(k)}\right)E\left(r^{(k)}\right)}{r^{(k)}}\left(\nu\left(r^{(k)}\right)+1\right),$$
$$c_4^{(k)}=\rho\left(r^{(k)}\right)h\left(r^{(k)}\right)\left(r^{(k)}\right)^2\left(1-\left(\nu\left(r^{(k)}\right)\right)^2\right)\omega^2-r^{(k)}\left(\nu\left(r^{(k)}\right)+1\right)\frac{\mathrm{d}\left(E(r)h(r)\alpha(r)T(r)\right)}{\mathrm{d}r}\Big|_{r=r^{(k)}},$$
$$c_5^{(k)}=\frac{1}{\left(h\left(r^{(k)}\right)\right)^2}\frac{\mathrm{d}\left(rE(r)(h(r))^3\right)}{\mathrm{d}r}\Big|_{r=r^{(k)}}+\frac{2\nu\left(r^{(k)}\right)c_1^{(k)}}{1-\left(\nu\left(r^{(k)}\right)\right)^2}\frac{\mathrm{d}\nu(r)}{\mathrm{d}r}\Big|_{r=r^{(k)}},$$
$$c_6^{(k)}=\frac{\nu\left(r^{(k)}\right)}{r^{(k)}\left(h\left(r^{(k)}\right)\right)^2}\frac{\mathrm{d}\left(rE(r)(h(r))^3\right)}{\mathrm{d}r}\Big|_{r=r^{(k)}}+h\left(r^{(k)}\right)E\left(r^{(k)}\right)\left(1+\frac{2\left(\nu\left(r^{(k)}\right)\right)^2}{1-\left(\nu\left(r^{(k)}\right)\right)^2}\right)\frac{\mathrm{d}\nu(r)}{\mathrm{d}r}\Big|_{r=r^{(k)}}$$
$$-\frac{h\left(r^{(k)}\right)E\left(r^{(k)}\right)}{r^{(k)}}\left(\nu\left(r^{(k)}\right)+1\right),$$
$$c_7^{(k)}=6\left(\nu\left(r^{(k)}\right)-1\right)\frac{r^{(k)}E\left(r^{(k)}\right)k_s}{h\left(r^{(k)}\right)},$$
$$c_8^{(k)}=\frac{dc_1}{dr}\Big|_{r=r^{(k)}}-\frac{c_1^{(k)}}{\left(1+\nu\left(r^{(k)}\right)\right)}\frac{d\nu(r)}{dr}\Big|_{r=r^{(k)}},$$
$$c_9^{(k)}=2\left(\nu\left(r^{(k)}\right)+1\right)r^{(k)}q_z,$$

in which $c_i^{(k)}$, $(i=1,2,\ldots,9)$ are functions of $r^{(k)}$. Using the semi-analytical method to solve the differential equation for temperature and system of displacement differential equations (17), we find

$$\left.\begin{aligned} T^{(k)} &= B_1^{(k)} + B_2^{(k)}\mathrm{e}^{-G_1^{(k)}r}, \\ u_0^{(k)} &= X_1^{(k)}exp\left(\lambda_1^{(k)}r\right) + X_2^{(k)}exp\left(\lambda_2^{(k)}r\right) - \frac{c_4^{(k)}}{c_3^{(k)}}, \\ \psi^{(k)} &= X_3^{(k)}exp\left(\lambda_3^{(k)}r\right) + X_4^{(k)}exp\left(\lambda_4^{(k)}r\right) + X_5^{(k)}exp\left(\lambda_5^{(k)}r\right) + A_1, \\ w^{(k)} &= -\frac{X_3^{(k)}}{\lambda_3^{(k)}}exp\left(\lambda_3^{(k)}r\right) - \frac{X_4^{(k)}}{\lambda_4^{(k)}}exp\left(\lambda_4^{(k)}r\right) - \frac{X_5^{(k)}}{\lambda_5^{(k)}}exp\left(\lambda_5^{(k)}r\right)A_2 - rA_3 + X_6^{(k)} \end{aligned}\right\} \tag{18}$$

where $\lambda_1^{(k)}$, $\lambda_2^{(k)}$ are the roots of $c_1^{(k)}\lambda^2 + c_2^{(k)}\lambda + c_3^{(k)} = 0$; $\lambda_4^{(k)}$, $\lambda_5^{(k)}$ are the roots of $c_1^{(k)}\lambda^2 + c_5^{(k)}\lambda + c_6^{(k)} = 0$; and

$$G_1^{(k)} = \left(\frac{1}{r} + \frac{1}{h(r)}\frac{\mathrm{d}h(r)}{\mathrm{d}r} + \frac{1}{k_T(r)}\frac{\mathrm{d}k_T(r)}{\mathrm{d}r}\right)\Big|_{r=r^{(k)}}, \qquad \lambda_3^{(k)} = -\frac{c_8^{(k)}}{c_1^{(k)}},$$

$$A_1 = \frac{c_7^{(k)}c_9^{(k)}}{c_6^{(k)}c_8^{(k)}}, \qquad A_2 = \frac{1}{c_7^{(k)}}\left(\frac{c_8^{(k)}\left(c_8^{(k)} - c_5^{(k)}\right)}{c_1^{(k)}} + c_6^{(k)} + c_7^{(k)}\right), \qquad A_3 = \frac{c_9^{(k)}\left(c_6^{(k)} + c_7^{(k)}\right)}{c_8^{(k)}c_6^{(k)}},$$

here $B_1^{(k)}$, $B_2^{(k)}$, $X_1^{(k)}$, $X_2^{(k)}$, $X_3^{(k)}$, $X_4^{(k)}$, $X_5^{(k)}$ and $X_6^{(k)}$ are the unknowns of differential equations for kth subsection. The thermal and displacements solution (18) is correct at

$$r^{(k)} - \frac{s^{(k)}}{2} \le r \le r^{(k)} + \frac{s^{(k)}}{2}, \tag{19}$$

where $s^{(k)}$ and $r^{(k)}$ are the radial width and the mean radius of the kth subsection.

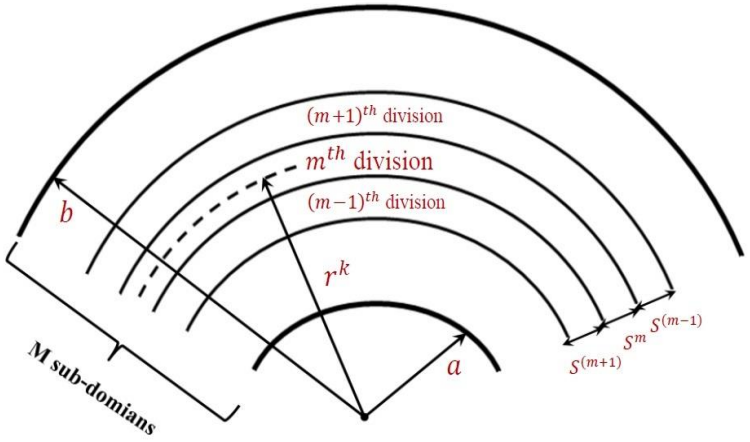

Fig. 2. Subsection of the radial domain by semi-analytical technique.

Continuity relations for temperature and displacements for two neighboring subsections can be written as:

$$\Phi^{(k)}\Big|_{r=r^{(k)}+\frac{s^{(k)}}{2}} = \Phi^{(k+1)}\Big|_{r=r^{(k+1)}-\frac{s^{(k+1)}}{2}}, \tag{20}$$

here Φ takes the following values T, $\frac{\mathrm{d}T}{\mathrm{d}r}$, u_z, $\frac{\mathrm{d}u_z}{\mathrm{d}r}$, M_r, Q_r, and σ_r.

Continuity relations (20) with the three different status of boundary conditions (14), (15), and (16) individually yields a linear system of unknowns $B_i^{(k)}$ and $X_j^{(k)}$ $(i = 1,2,\ j = 1,\ldots,5,\ k = 1,2,\ldots,m)$. After obtaining the solution, the temperature and displacements at each subsection become known. To reduce the error coefficient and obtain highly accurate numerical results, we can divide the radial domain into a larger number of subsections.

For appropriateness, we assume the following dimensionless notations

$$\overline{r} = \frac{r}{b}, \quad \overline{r}_a = \frac{a}{b}, \quad \overline{h} = \frac{h}{h_0}, \quad \overline{u}_0 = \frac{u_0}{b}, \quad \overline{\psi} = \frac{\psi}{b}, \quad \overline{w} = \frac{w}{b}, \quad \overline{\omega} = \frac{\omega}{h_0E_a}, \quad \overline{q}_z = \frac{q_z}{k_sh_0E_a},$$

$$\overline{E}(\overline{r}) = \frac{E(\overline{r})}{E^{(a)}} = (\delta_1 - 1)\left(\frac{\overline{r} - \overline{r}_a}{1 - \overline{r}_a}\right)^n + 1 - \frac{\beta}{2}(\delta_1 + 1),$$

$$\overline{\rho}(\overline{r}) = \frac{\rho(\overline{r})}{\rho^{(a)}} = (\delta_2 - 1)\left(\frac{\overline{r} - \overline{r}_a}{1 - \overline{r}_a}\right)^n + 1 - \frac{\beta}{2}(\delta_2 + 1),$$

$$\overline{\alpha}(\overline{r}) = \frac{\alpha(\overline{r})}{\alpha^{(a)}} = (\delta_3 - 1)\left(\frac{\overline{r} - \overline{r}_a}{1 - \overline{r}_a}\right)^n + 1 - \frac{\beta}{2}(\delta_3 + 1),$$

$$\overline{k}(\overline{r}) = \frac{k(\overline{r})}{k^{(a)}} = (\delta_4 - 1)\left(\frac{\overline{r} - \overline{r}_a}{1 - \overline{r}_a}\right)^n + 1 - \frac{\beta}{2}(\delta_4 + 1),$$

where $\delta_1 = \frac{E^{(b)}}{E^{(a)}}$, $\delta_2 = \frac{\rho^{(b)}}{\rho^{(a)}}$, $\delta_3 = \frac{\alpha^{(b)}}{\alpha^{(a)}}$, and $\delta_4 = \frac{k^{(b)}}{k^{(a)}}$ then removing the bar symbols for simplicity.

5. Viscoelastic solution for gradient porous disk

Assume that viscoelastic material recognized by $E^{(b)}, \nu^{(b)}$ or by bulk modulus K and it is supposed to be unrelaxed, i.e., $K = constant$ and $\widehat{\varpi}$ is the dimensionless kernel of the relaxation function which is associated with the corresponding Poisson's ratio by formulation

$$E^{(b)} = \frac{9K\widehat{\varpi}}{2+\widehat{\varpi}}, \quad \nu^{(b)} = \frac{1-\widehat{\varpi}}{2+\widehat{\varpi}}, \tag{21}$$

where $K = \xi E^{(a)}$, then the gradient relation (2) takes the form

$$\left.\begin{aligned} E(r) &= \left(\frac{9\xi\widehat{\varpi}}{2+\widehat{\varpi}} - 1\right)\left(\frac{\overline{r}-\overline{r_a}}{1-\overline{r_a}}\right)^n + 1 - \frac{\beta}{2}\left(\frac{9\xi\widehat{\varpi}}{2+\widehat{\varpi}} + 1\right), \\ \nu(r) &= \left(\frac{1-\widehat{\varpi}}{2+\widehat{\varpi}} - \nu^{(a)}\right)\left(\frac{\overline{r}-\overline{r_a}}{1-\overline{r_a}}\right)^n + \nu^{(a)} - \frac{\beta}{2}\left(\frac{1-\widehat{\varpi}}{2+\widehat{\varpi}} + \nu^{(a)}\right) \end{aligned}\right\} \tag{22}$$

To resolve the quasi-static issue of linear theory for porous FG viscoelastic disk, we employ a technique of reducing the non-homogenous porous FG viscoelastic disk to a series of successive homogenous ones [40, 41].

Displacements can be taken as constant functions in elastic components and operator functions of time in viscoelastic components. Overall, $w(r)$, $N_r(r)$, $M_r(r)$ and $Q_r(r)$ written by Illyushin's approximation technique, of unified shape

$$f(r, z, \widehat{\varpi}) = \sum_{i=1}^{5} y_i(r, z)\varphi_i(\widehat{\varpi}), \tag{23}$$

where $f(r, z, \widehat{\varpi})$ is one of the functions $w(r)$, $N_r(r)$, $M_r(r)$ and $Q_r(r)$ and $\varphi_i(\widehat{\varpi})$ are several recognized kernels, structured based on the kernel $\widehat{\varpi}$ and might be selected in the format

$$\left.\begin{aligned} &\varphi_1 = 1, \quad \varphi_2 = \widehat{\varpi}, \qquad \varphi_3 = \widehat{\pi} = \frac{1}{\widehat{\varpi}}, \\ &\varphi_4 = \widehat{g_{\frac{1}{2}}}, \quad \varphi_5 = \widehat{g_2}, \quad \widehat{g_x} = \frac{1}{1+x\widehat{\varpi}}, x = \frac{1}{2}, 2 \end{aligned}\right\} \tag{24}$$

The coefficients $y_i(r, z)$, $(i = 1,2,..,5)$ get from the linear algebraic equations system

$$\left.\begin{aligned} l_{ij}y_j &= g_i, \\ l_{ij} &= \int_0^1 \varphi_i(\widehat{\varpi})\varphi_j(\widehat{\varpi})d\widehat{\varpi}, \\ g_i &= \int_0^1 f(r, z, \widehat{\varpi})\varphi_i(\widehat{\varpi})d\widehat{\varpi} \end{aligned}\right\} \tag{25}$$

Postulate the relaxation function

$$\varpi(t) = a_1 + b_1 \mathrm{e}^{-\alpha_1 t}, \tag{26}$$

where a_1, b_1, α_1 are constants specified through practical experience.

The Laplace-Carson transformation is known as

$$F(p) = p\int_0^\infty \mathrm{e}^{-px} f(x)\mathrm{d}x. \tag{27}$$

The transformation applied to specified functions $\pi(t)$ and $\mathrm{g}_x(t), (x = 0.5,2)$. Indicating that transformations of $\pi(t)$ and $\mathrm{g}_x(t)$ by π^* and g_x^* since $\varpi^* = a_1 + \frac{b_1 s}{s+\alpha_1}$ consequently

$$\left.\begin{aligned} \pi(t) &= \frac{1}{a_1}\left(1 - \frac{b_1}{a_1+b_1}\mathrm{e}^{-\frac{a_1\tau}{a_1+b_1}}\right), \quad \tau = \alpha_1 t, \\ \mathrm{g}_x(t) &= \frac{1}{1+xa_1}\left(1 - \frac{xb_1}{1+x(a_1+b_1)}\mathrm{e}^{-\frac{(1+xa_1)\tau}{1+x(a_1+b_1)}}\right), \quad x = 0.5,2, \end{aligned}\right\} \tag{28}$$

Equation (23) for a viscoelastic composite used to get the formulation $f(r, z, \widehat{\varpi})$ as function of (r, z, t). consequently so,

$$f(r, z, t) = y_1\omega(t) + y_2\int_0^1 \varpi(t-\tau)d\omega(\tau) + y_3\int_0^1 \pi(t-\tau)d\omega(\tau)$$
$$+y_4\int_0^1 \mathrm{g}_{\frac{1}{2}}(t-\tau)d\omega(\tau) + y_5\int_0^1 \mathrm{g}_2(t-\tau)d\omega(\tau)$$

or

$$f(r, z, t) = y_1\mathrm{q}(t) + y_2\int_0^1 \varpi(t-\tau)\mathrm{dq}(\tau) + y_3\int_0^1 \pi(t-\tau)\mathrm{dq}(\tau) + y_4\int_0^1 \mathrm{g}_{\frac{1}{2}}(t-\tau)\mathrm{dq}(\tau)$$
$$+y_5\int_0^1 \mathrm{g}_2(t-\tau)\mathrm{dq}(\tau). \tag{29}$$

Suppose the formulation of rotation velocity $\omega(t)$, and the vertical load $q_z(t)$ as

$$\omega(t) = \begin{cases} \omega_0 t & 0 \le t \le t_0 \\ \omega_0 H(t-t_0) & t \ge t_0 \end{cases}$$

$$q_z(t) = \begin{cases} q_0 t & 0 \le t \le t_0 \\ q_0 H(t-t_0) & t \ge t_0 \end{cases}$$

where $H(t)$ is the Heaviside unit step function and ω_0, t_0, q_0 are the initial values of rotation velocity, time, and vertical load sequentially. The formulation (29) is written as

$$f(r,z,t) = \omega_0 \sum_{j=1}^{5} y_j(r,z) V_j(t), \tag{30}$$

where

$$y_1 = \begin{cases} t & 0 \le t \le t_0 \\ H(t-t_0) & t \ge t_0 \end{cases}$$

$$y_2 = \begin{cases} -F_1(1) + 2a_1 t_0 & 0 \le t \le t_0 \\ a_1 + F_2(1) & t \ge t_0 \end{cases}$$

$$y_3 = \begin{cases} \dfrac{1}{a_1^2} F_1\left(\dfrac{a_1}{a_1+b_1}\right) & 0 \le t \le t_0 \\ \dfrac{1}{a_1}\left(1 - \dfrac{F_2\left(\frac{a_1}{a_1+b_1}\right)}{a_1+b_1}\right) & t \ge t_0 \end{cases}$$

$$y_4 = \begin{cases} \dfrac{2}{(2+a_1)^2}\left(F_1\left(\dfrac{2+a_1}{2+a_1+b_1}\right) - 2t_0\right) & 0 \le t \le t_0 \\ \dfrac{2}{(2+a_1)}\left(1 - \dfrac{F_2\left(\frac{2+a_1}{2+a_1+b_1}\right)}{(2+a_1+b_1)}\right) & t \ge t_0 \end{cases}$$

$$y_5 = \begin{cases} \dfrac{1}{(1+2a_1)^2}\left(2F_1\left(\dfrac{1+2a_1}{1+2a_1+2b_1}\right) - t_0\right) & 0 \le t \le t_0 \\ \dfrac{1}{(1+2a_1)}\left(1 - \dfrac{2F_2\left(\frac{1+2a_1}{1+2a_1+2b_1}\right)}{(1+2a_1+2b_1)}\right) & t \ge t_0 \end{cases}$$

here $F_1(y) = b_1 e^{-yt} + a_1 t_0 - b_1 e^{-y(t-t_0)}$, $F_2(y) = b_1 e^{-y(t-t_0)}$, and the other formulation gets it by substitution ω_0 by q_0.

6. Verification of numerical outputs of solid and annular FG porous disk

In this research, the analytical results were studied and the numerical results were verified for a viscous annular porous disk of exponentially varying thickness, which undergoes a gradient as a power function in its physical and thermal characteristics in radius direction. The disk is exposed to thermal and mechanical forces on the inner surface consisting of PZT-4 and the outer surface consisting of cadmium selenide. The numerical results for three different cases of solid disk and annular disk are divided to discuss influences of inhomogeneity and porosity as well as the effect of relaxation time in the case of viscous porous disk.

6.1 Status 1: Circular solid porous disk

To study the case of a circular viscous solid porous disk, we assume that the boundary conditions on the disk satisfy equation (14). We first begin by studying the effect of heterogeneity, then porosity, and then relaxation time for the viscous porous disk.

Figure 3 studies the result of bending on a solid porous circular disk of variable thickness and demonstrates the effect of the inhomogeneity parameter at $n = 2,4,6,8$ and $n \longrightarrow \infty$ in the direction of the radius. Fig. 3a shows the value of displacement $\overline{w}$ for several values of inhomogeneity parameter n. It is clear in the image that displacement $\overline{w}$ value increased with the increase in radius, achieving zero at the outer radius $\overline{r} = 1$ and fulfilling the boundary conditions. The figure furthermore presents that the minimum value of displacement $\overline{w}$ occurs at $n = 4$ along the radius. Fig. 3b presents the value of the force per unit length $\bar{N}_r$ and the figure shows that the value of the force $\bar{N}_r$ begins to increase from the center of the disk until $\overline{r} = 0.1$ and then begins to decrease until the outer surface of the disk $\overline{r} = 1$, achieving a value of zero, which corresponds to the boundary conditions. It is clear from the figure that the value of the force $\bar{N}_r$ increases with the increase in the value of the inhomogeneity parameter n, as its lowest value is done at $n = 2$ and its highest value is done when $n \longrightarrow \infty$. The value of the moment per unit length $\bar{M}_r$ was illustrated in Fig. 3c, it is clear that the value of the moment $\bar{M}_r$ is zero at the center of the disc, then it begins to decrease until approximately the middle of the thickness, and then it begins to increase until the outer surface of the disc, achieving zero and agreeing with the boundary conditions on the external surface. Fig. 3d displayed the value of the transverse shear resultant $\bar{Q}_r$, from which it appears that all curves are almost identical along the disk at numerous values of inhomogeneity parameter n. The value of $\bar{Q}_r$ starts from zero at the center of the disk according to the boundary conditions and then begins to increase until the external surface of the disk. Fig. 3e studies the temperature distribution along the disk diameter and shows the temperature curves with changing radius at different values of the inhomogeneity parameter n, fulfilling the boundary conditions.

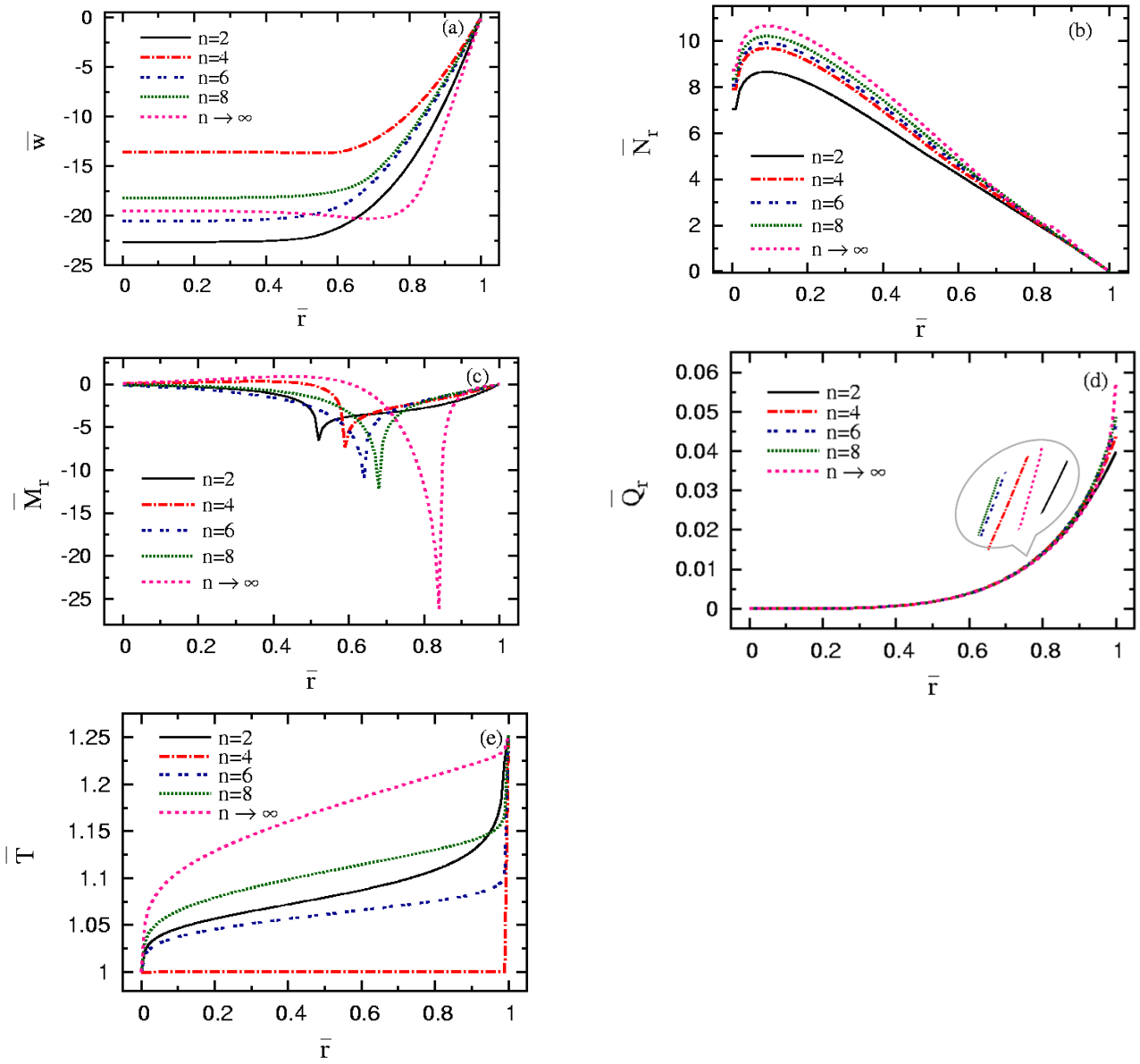

Fig. 3. Non-dimensional pending components and temperature at different inhomogeneity factor n with porosity parameter $\beta = 0.1$ in circular solid porous disk.

Figure 4 presents the bending components and temperature at different values of the porosity coefficient $\beta = 0,0.1,0.3,0.5$ and $\beta = 0.7$ with constant value of inhomogeneity parameter $n = 10$ in the case of the porous circular disc of variable thickness. The value of displacement $\overline{w}$ at various values of the porosity coefficient β was explained and presented in Fig. 4a. It is clear from the drawing that the displacement $\overline{w}$ value starts from the center of the disk, $\overline{r} = 0$, heading to the outer surface, achieving a value of zero at $\overline{r} = 1$, and conforming to the boundary conditions.

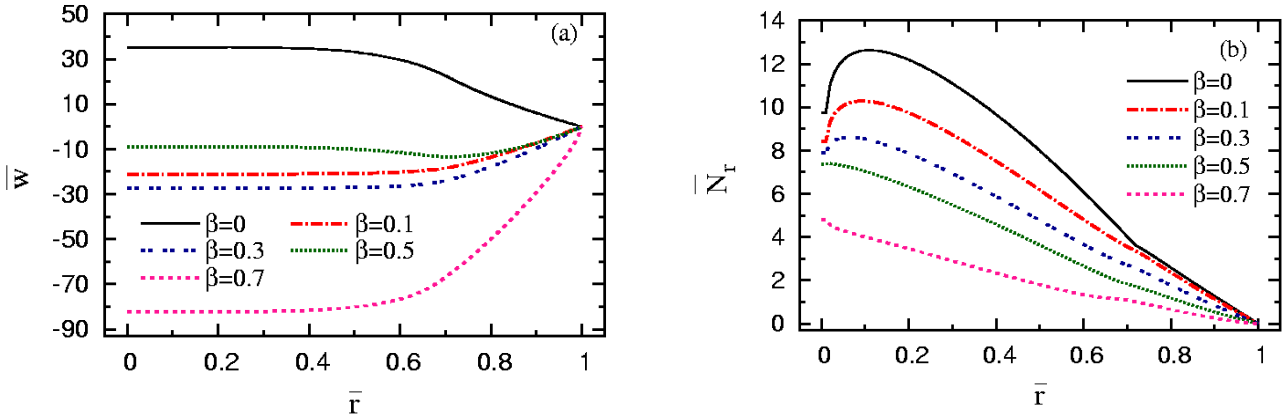

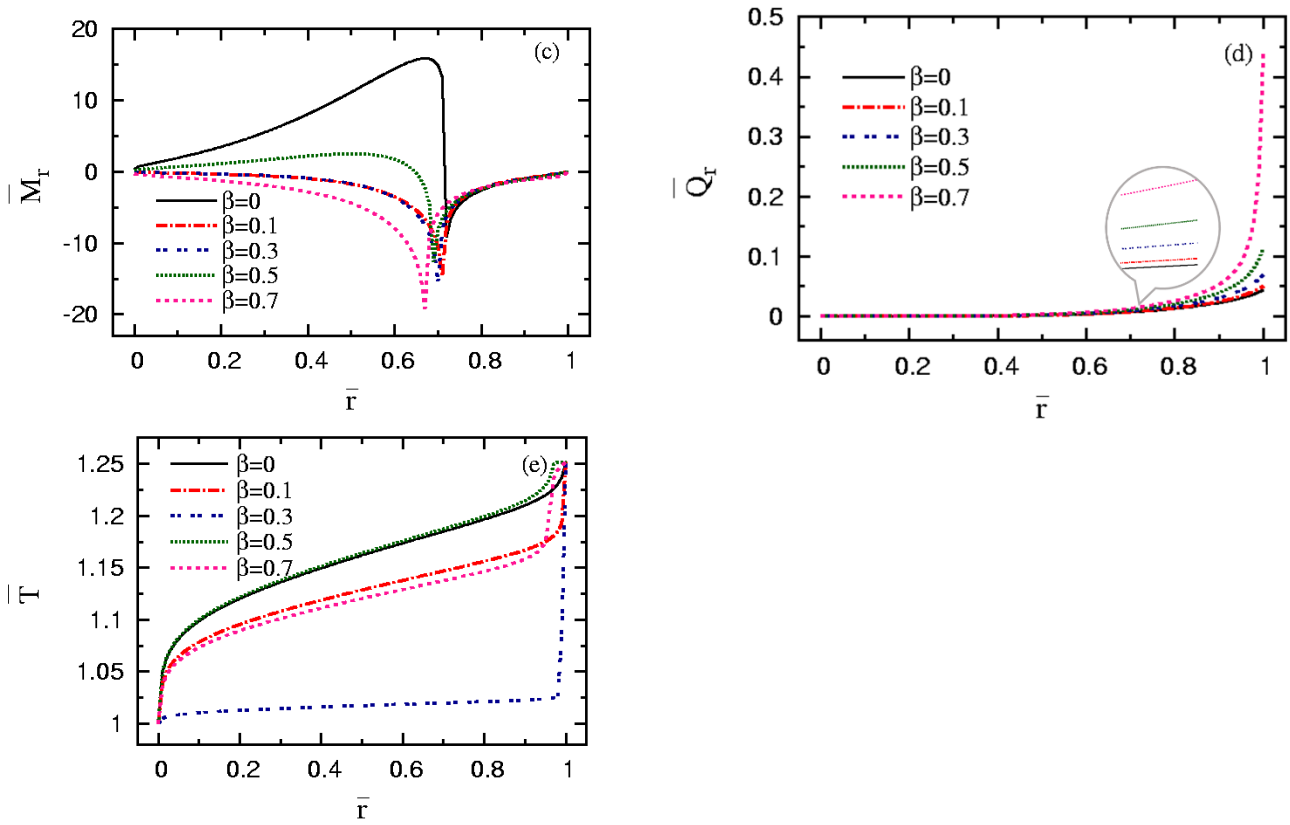

Fig. 4. Non-dimensional pending components and temperature at various values of porosity and $n = 10$ in circular solid porous disk.

Fig. 4b displays the value of the forces $\bar{N}_r$ per unit length at different values of porosity β and shows that the value of the force $\bar{N}_r$ decreases with an growth in the porosity factor β. The highest strength value was achieved in the case of the non-porous disc $\beta = 0$. Fig. 4c lights the moments per unit length $\bar{M}_r$ at different values of β, and it is clear that $\bar{M}_r$ start from zero, then decrease until the middle of the thickness at values of $\beta = 0.1,0.3,0.5$ and $\beta = 0.7$ then they begin to increase until the outer surface at $\bar{r} = 1$, achieving the value zero. In the case of a non-porous disc $\beta = 0$, the curve starts from zero at the center of the disc, then begins to increase until the middle of the thickness of the disc, then decreases towards the outer surface $\bar{r} = 1$, fulfilling the boundary conditions $\bar{M}_r = 0$ at $\bar{r} = 1$. As for $\bar{Q}_r$, its rate of change with the change in porosity coefficient β was shown in Fig. 4d . It appears that the curves match roughly, achieving a value of zero at the center of the disk. From the curves, the value of $\bar{Q}_r$ increases with the increase in the porosity coefficient β along the length of the disk. Fig. 4e illustrates temperature distribution $\bar{T}$ at several values of the porosity coefficient β, fulfilling the limit conditions for the temperature at the center of the disk and at the outer surface of the disk.

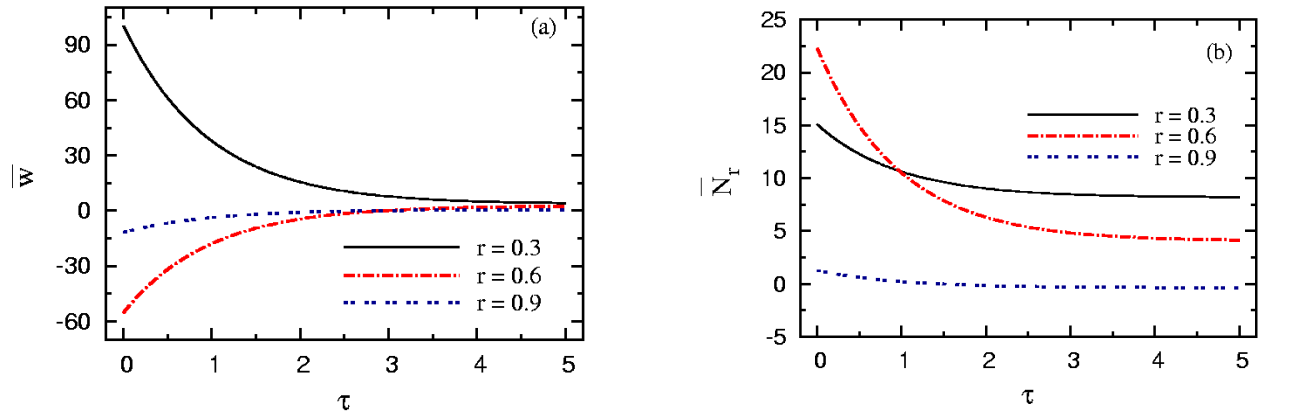

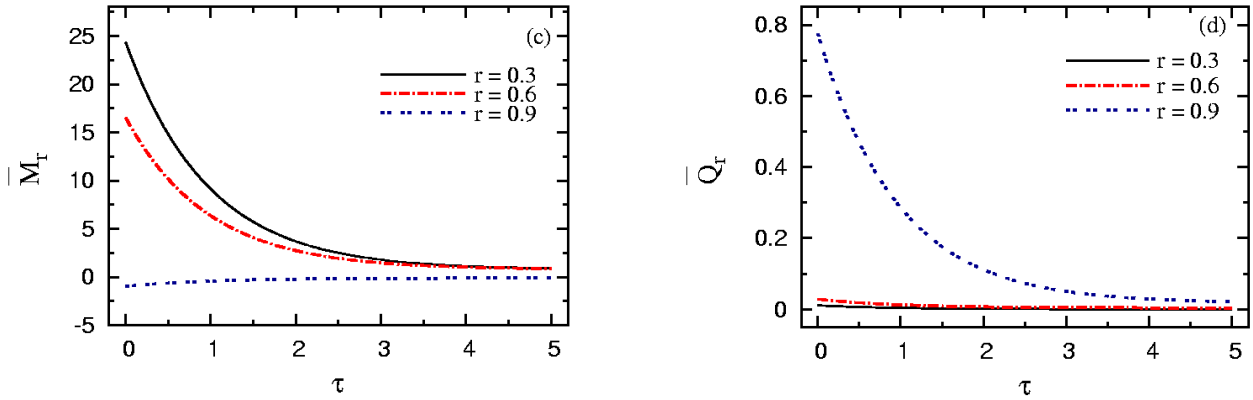

Fig. 5. Pending components along time parameter of viscoelastic FG circular solid porous disk.

Figure 5 clarifies the value of $\overline{w}$, $\overline{N}_r$, $\overline{M}_r$, and $\overline{Q}_r$ at multiple positions of the disc, $\overline{r} = 0.3{,}0.6$ and 0.9 with the relaxation time τ to examine the influence of the time factor on bending components. It is clear from the images that the curves increase or decrease starting from $\tau = 0$ until they reach a state of stability at a specific value of the relaxation time $\tau = 3.5$.

6.2 Status 2: Mounted free hollow porous disk

To study the second status of a hollow porous disk of variable thickness, we assume that the disk is fixed at the internal surface, $\overline{r} = 0.2$, and free to move at the outer surface, $\overline{r} = 1$. The study aims to know the influence of inhomogeneity parameter n in Fig. 6 and the effectiveness of the porosity factor β in Fig. 7, as well as to know the effect of the time factor on the hollow porous disk in Fig. 8.

In Fig. 6, the effectiveness of the inhomogeneity parameter n on bending and temperature components appears very clearly. It is clear from Fig. 6a that the displacement $\overline{w}$ along the thickness fulfills the boundary conditions of zero at the inner radius $\overline{r} = 0.2$. Also, the values of all curves, with the change in the value of the inhomogeneity parameter n, begin to increase from the inner surface at $\overline{r} = 0.2$ until $\overline{r} = 1$. As for Fig. 6b, the effect of force $\overline{N}_r$ per unit length with a value of zero on the outer surface $\overline{r} = 1$ appears, identical to the boundary conditions. It is clear from the drawing that the force $\overline{N}_r$ value begins to decrease in the direction of the radius. Fig. 6c shows the value of the moments $\overline{M}_r$ per unit length in the direction of the radius with numerous values of the inhomogeneity parameter n. The value of the moments $\overline{M}_r$ begins to decrease from the inner surface, $\overline{r} = 0.2$, until approximately the middle of the disk, then it begins to increase, achieving a value of zero on the external surface of the disk, $\overline{r} = 1$. The influence of inhomogeneity parameter n on $\overline{Q}_r$ is clearly evident from Fig. 6d where the value begins to increase from $\overline{r} = 0.2$ until it becomes zero at $\overline{r} = 1$, matching the boundary conditions. It is also clear that the value of $\overline{Q}_r$ decreases with the increase in the inhomogeneity parameter n, as it achieves its lowest value when $n \longrightarrow \infty$, and its highest value of $\overline{Q}_r$ is achieved in the non-porous disk, that is when $\beta = 0$. The effectiveness of inhomogeneity parameter n on the thermal distribution is shown in Fig. 6e, which shows the effect of temperature $\overline{T}$ by variation value of inhomogeneity parameter n, achieving the boundary conditions for temperature parameter n on the thermal distribution is shown in Fig. 6e, which shows the effect of temperature $\overline{T}$.

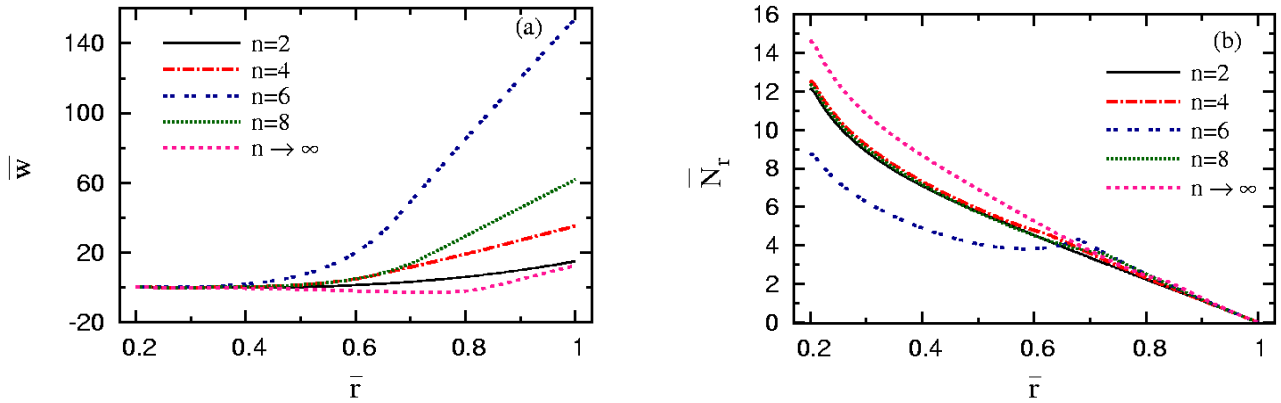

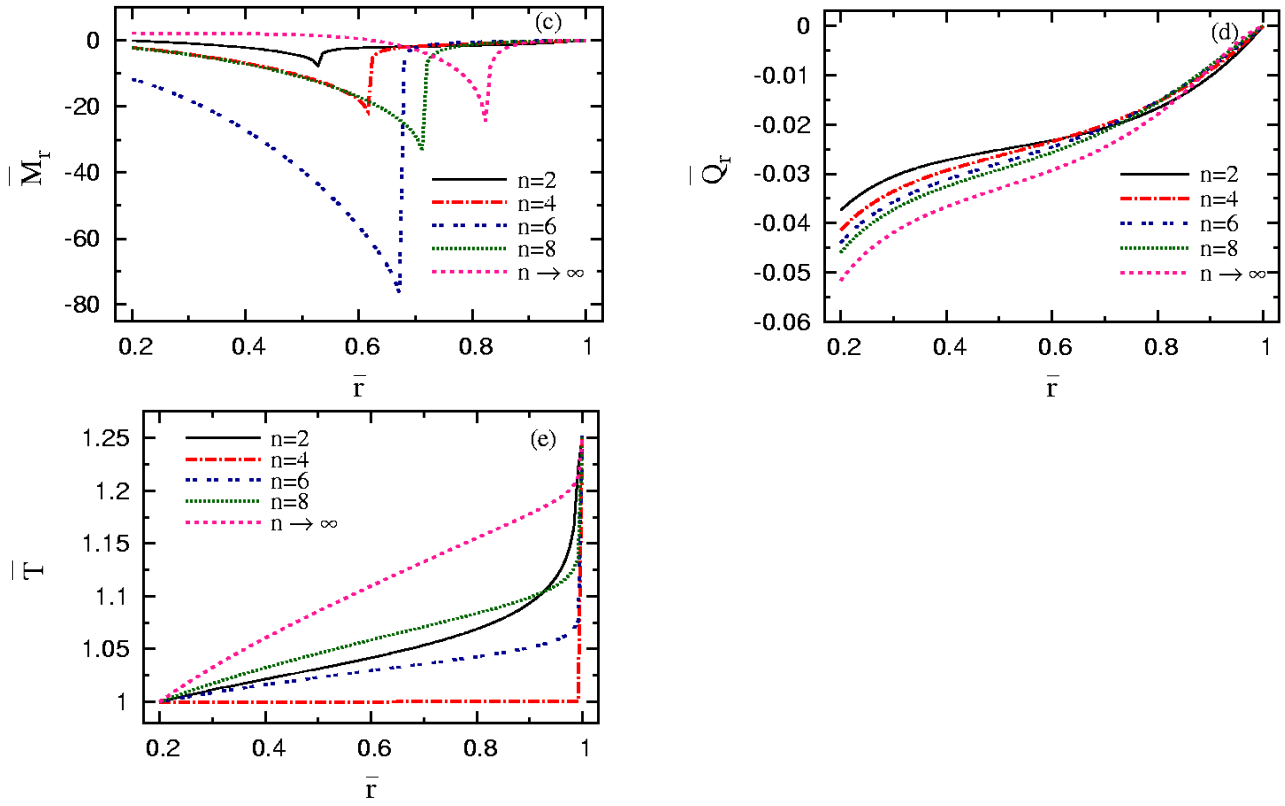

Fig. 6 Non-dimensional pending components and temperature at different inhomogeneity factor n with porosity parameter $\beta = 0.1$ in mounted free hollow porous disk.

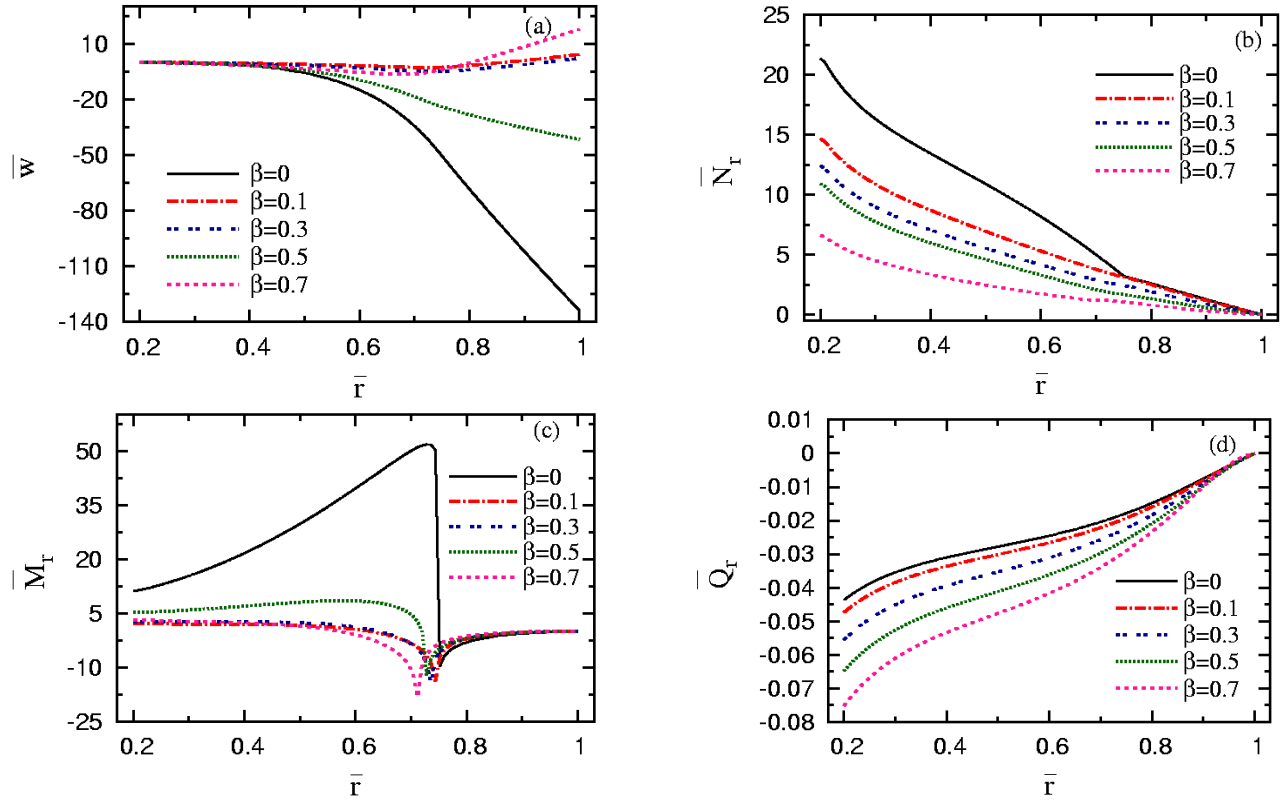

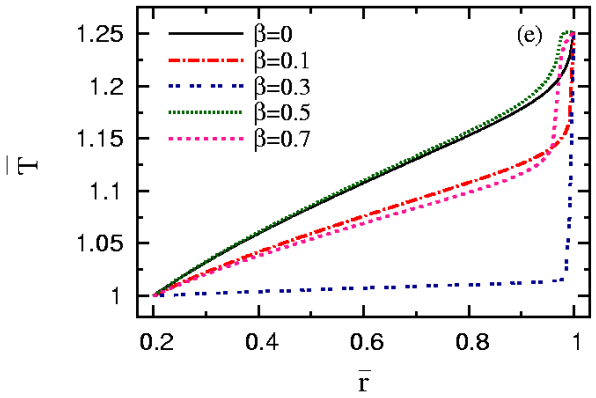

Fig. 7 Non-dimensional pending components and temperature at various values of porosity and $n = 10$ in the mounted free hollow porous disk.

Figure 7 shows the effectiveness of the porosity coefficient on the hollow porous disk of variable thickness, with various values of the porosity coefficient $\beta = 0.1,0.3,0.5,0.7$ in the case of the porous disk and $\beta = 0$ in the case of the non-porous disk. In the Fig. 7a, the displacement $\overline{w}$ study with numerous values of the porosity coefficient in the direction of the radius shows that the largest value of the displacement $\overline{w}$ was achieved in the case of $\beta = 0.7$, while the smallest value of the displacement $\overline{w}$ was achieved in the case of the non-porous disk, $\beta = 0$. Therefore, the displacement $\overline{w}$ is increasing as the porosity coefficient grows. The exact opposite appears in Fig. 7b to study the effectiveness of changing the porosity parameter β on the force $\overline{N}_r$ per unit length, where the highest value of the force $\overline{N}_r$ is achieved in the case of the non-porous disk, $\beta = 0$, and the lowest value of the force $\overline{N}_r$ is achieved in the case of $\beta = 0.7$. Fig. 7c shows the value of the moment $\overline{M}_r$ per unit length, and it is clear from the curves that the gradation value of the porosity coefficient β had a significant effect until $\overline{r} = 0.75$, then the curves began to match. The value of $\overline{Q}_r$ with the change in the porosity factor β was shown in Fig. 7.d, and it is clear from it that there is an inverse relationship between the change in the porosity factor β, as the value of the porosity factor β increases, the value of $\overline{Q}_r$ decreases. The result of the effect of the porosity factor β on temperature appears in Fig. 7e, and it shows a clear effect on the temperature $\overline{T}$ curves in the radial direction.

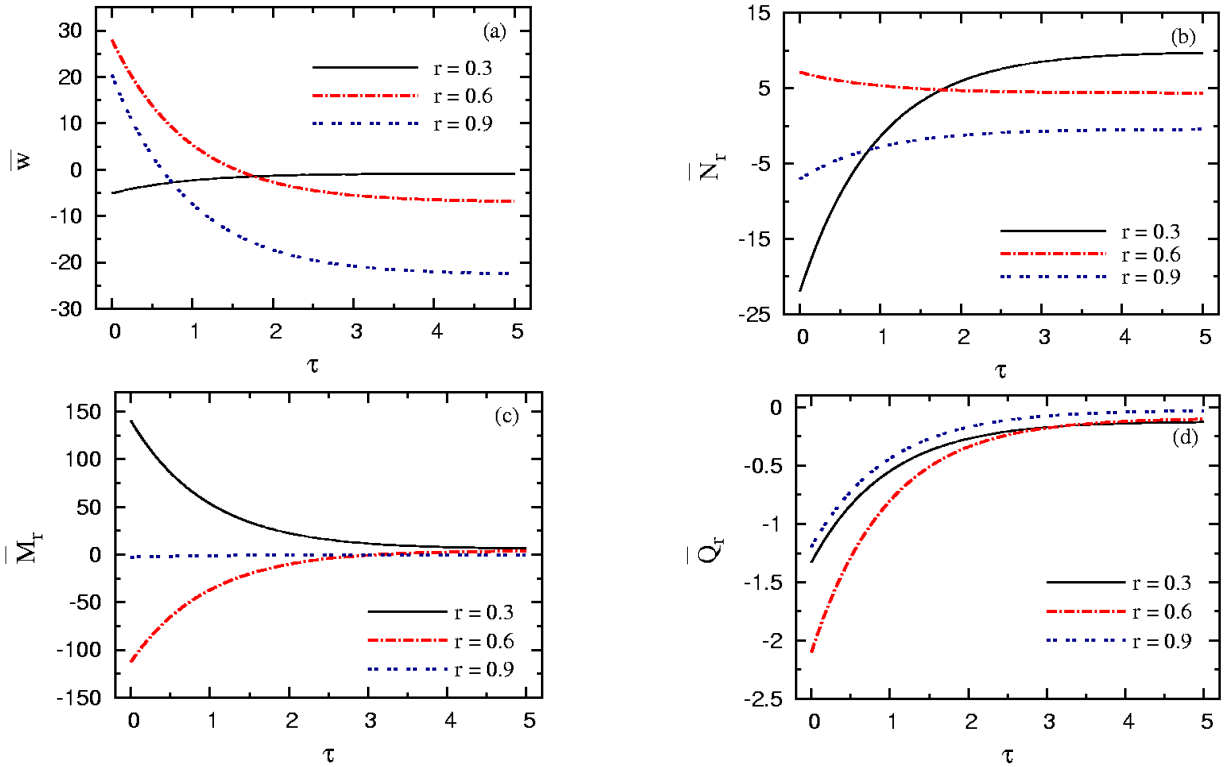

Fig. 8. Pending components along time parameter of viscoelastic FG mounted free hollow porous disk.

A study of the impact of the time parameter on the porous, viscous hollow disc of variable thickness appears in Fig. 8, from which it is clear that all the bending components that need to be studied tend to reach a state of stability after some time $\tau = 0.35$ to represent a state of equilibrium for a viscous disk.

6.3 Status 3: Mounted hollow supported cased porous disk

The case of the current study is the case of a mounted hollow supported cased porous disk fixed from the inside and outside to discuss the impact of the inhomogeneity parameter n, porosity β, and relaxation time τ on the porous disk in Figures 9 and 10, respectively.

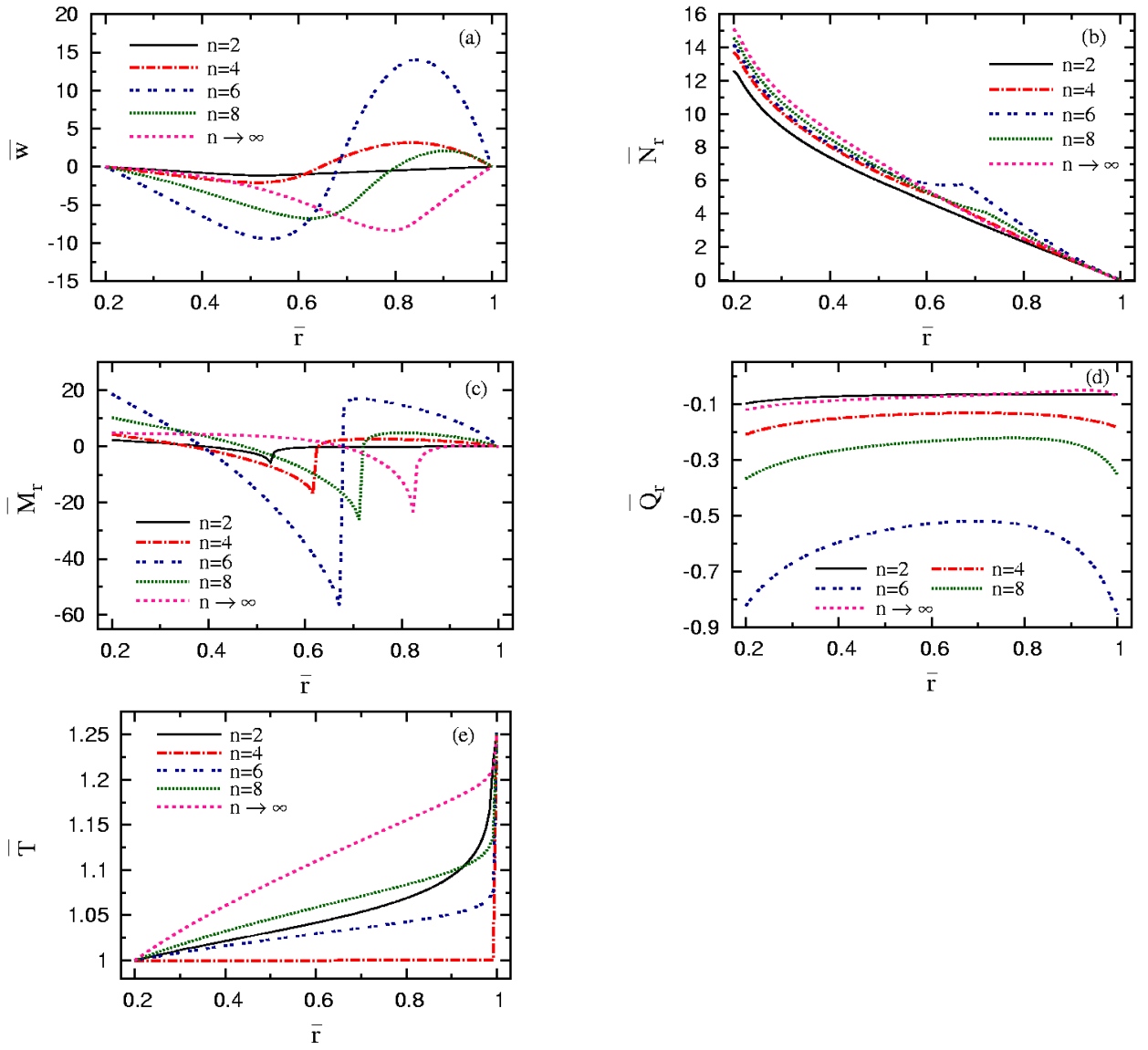

Fig. 9. Non-dimensional pending components and temperature at different inhomogeneity factor n with porosity parameter $\beta = 0.1$ in the mounted hollow supported cased porous disk.

In Fig. 9, the effect of inhomogeneity parameter n of different values at $n = 2,4,6,8$ and $n \to \infty$ on the bending components of the porous disk is studied. It is clear from Fig. 9a that the displacement $\overline{w}$ for numerous values of n are achieved in the internal and external surfaces of the disk. Fig 9b shows the effect of n on the force $\overline{N}_r$ in which the lowest value of $\overline{N}_r$ is achieved when $n = 2$. The moment $\overline{M}_r$ are displayed in Fig. 9c, in which the curves are clearly affected by the inhomogeneity parameter n. The value zero is achieved on the outer surface, which is consistent with the boundary conditions. Fig. 9d shows the transverse shear resultant value $\overline{Q}_r$ with the variation of the inhomogeneity parameter n, and it is clear from it that the lowest value of $\overline{Q}_r$ is achieved in the case $n = 6$. Fig. 9e matches Fig. 6e, and it displays the effectiveness of the inhomogeneity parameter n on temperature.

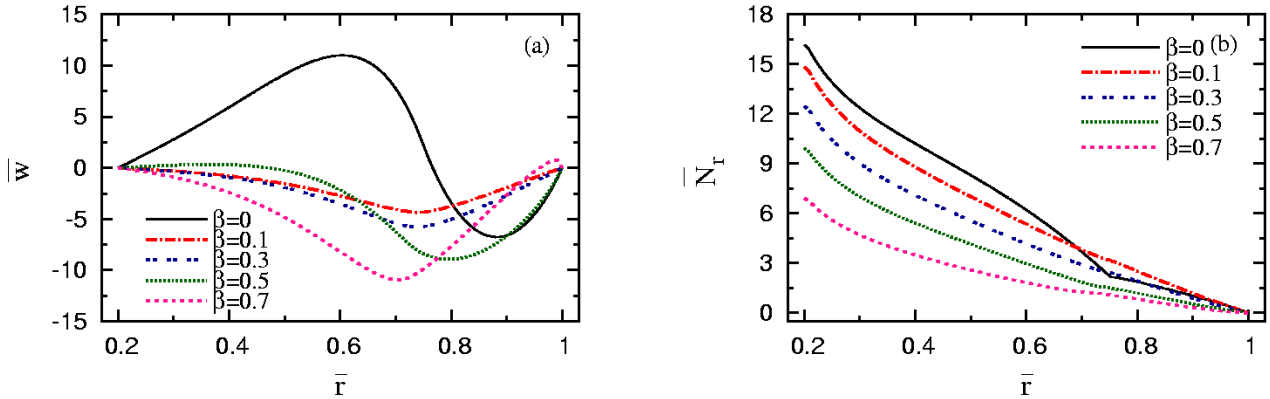

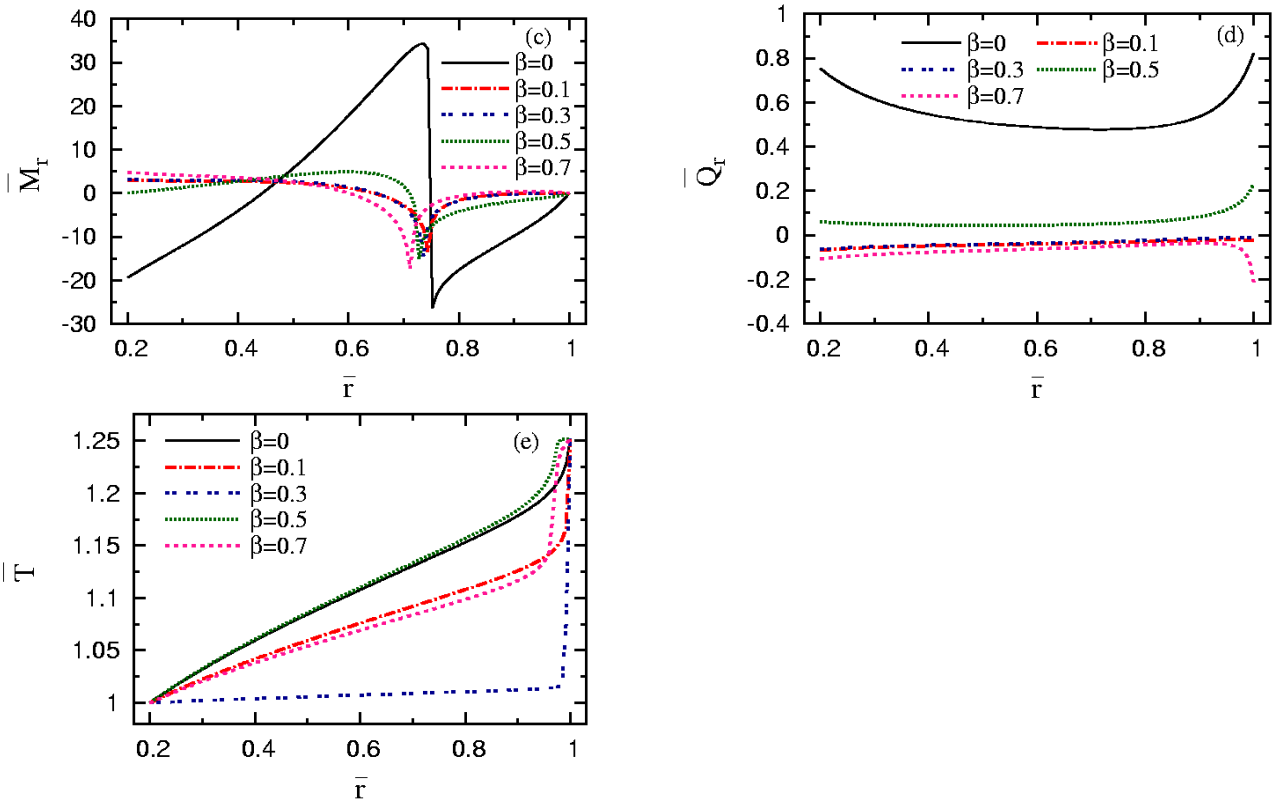

Fig. 10. Non-dimensional pending components and temperature at various values of porosity and $n = 10$ in the mounted hollow supported cased porous disk.

Fig. 10 studies the effectiveness of the porosity coefficient on the bending and temperature components. Fig. 10a shows the value of the behavior of the displacement $\overline{w}$ with a change in the porosity coefficient β. The displacement $\overline{w}$ achieves a value of zero at the inner and outer surfaces of the disk following the boundary conditions. Fig. 10b presents the influence of the porosity coefficient β on the force $\overline{N}_r$, and it is clear that the lowest value of the force $\overline{N}_r$ occurs when $\beta = 0.7$. In Fig. 10c, the moment $\overline{M}_r$ are displayed, and it is clear that the curves match significantly with the difference in the value of the porosity coefficient β in the case of the porous disk, while in the case of the non-porous disk $\beta = 0$, the value of the moment $\overline{M}_r$ in the direction of the radius varies greatly. In Fig. 10.d, the value of $\overline{Q}_r$ was shown which achieves the highest value in status of the non-porous disk when $\beta = 0$. As the value of the porosity factor β grows, the value of $\overline{Q}_r$ decreases. Figure 10e matches Fig. 7d, and it presents the influence of porosity coefficient β on temperature $\overline{T}$.

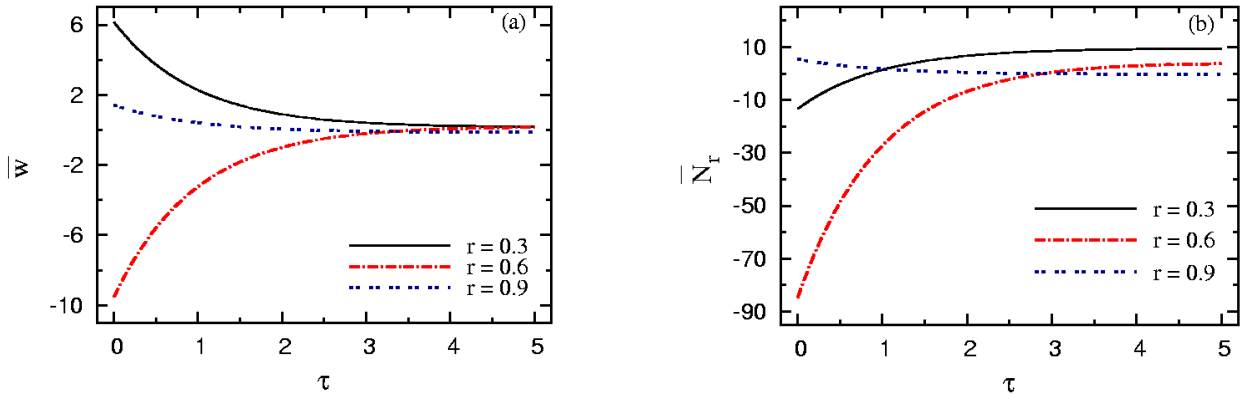

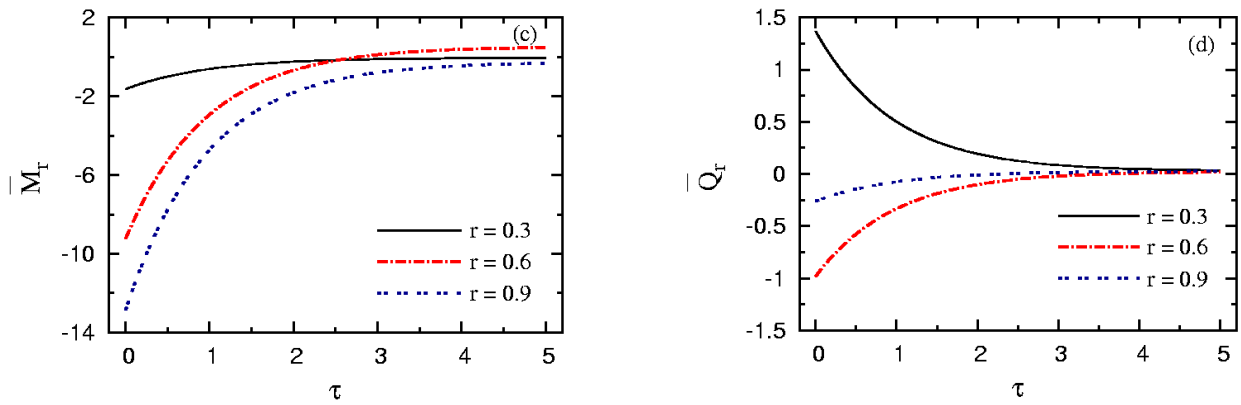

Fig. 11. Pending components along time parameter of viscoelastic FG mounted hollow supported cased porous disk.

Figure 11 studies the impact of the relaxation time parameter on bending components in the viscous porous disk. The results of Fig. 11 agree with those in Figs. 5 and 8, where the bending components reach a state of stability after a constant time rate $\tau = 3.5$.

7. Fundamental difference in results between a porous and a non-porous disk

To find out the fundamental differences in the numerical results for the FG exponentially porous disc, a comparison was presented in the numerical results for three special statuses of the variable thickness porous disc, and the results of the bending components were tabulated for several values of the inhomogeneity parameter $n = 5,10,20$ and at numerous positions $\overline{r} = 0.3,0.5,0.7$ of the porous disc in the direction of the radius. The results and comparison in the case of the porous disk $\beta = 0.1$ and the non-porous disk $\beta = 0$ are shown in Table 2 as follows.

7.1 Status 1: Circular solid porous disk

It can be seen from Table 2 in status of the porous solid circular disk as follows

- The largest value of force per unit length $\overline{N}_r$ is achieved in the status of a non-porous disk, while the largest value of transverse shear resultant $\overline{Q}_r$ is achieved in the case of a porous disk at various values of inhomogeneity parameter n and different positions.
- The numerical results for the displacement $\overline{w}$ differ in the porous and non-porous disk, as the displacement $\overline{w}$ achieves its highest value at $n = 10,20$ in the case of the non-porous disk and its highest value is achieved at $n = 5$ in the status of the porous disk.
- The value of moments per unit length $\overline{M}_r$ reaches the highest value in the non-porous disk at $n = 10$ and the highest value is achieved in the porous disk at $n = 5,20$.

7.2 Status 2: Mounted free hollow porous disk

The numerical results in the comparison between the porous disk and the non-porous disk differed from the first status, as it turns out that

- The non-porous disc achieves the highest results for bending components $\overline{N}_r$, $\overline{M}_r$, $\overline{Q}_r$ at all values of the inhomogeneity parameter n along the radial direction, while achieving the lowest value for displacement $\overline{w}$.

7.3 Status 3: Mounted hollow supported cased porous disk

- The non-porous disc achieves the highest values of displacement $\overline{w}$, force per unit length $\overline{N}_r$ and transverse shear resultant $\overline{Q}_r$ at all values of the inhomogeneity parameter n and different positions of the disk.
- The value of the moments per unit length $\overline{M}_r$ in status of the porous disk and the non-porous disk varied greatly depending on the inhomogeneity parameter and the radius value.

Table 2. The fundamental difference in results between a porous and a non-porous

Case	Variable	$\bar{r}$	Perfect FGPM ($\beta = 0$)			Porous FGPM ($\beta = 0.1$)		
			$n = 5$	$n = 10$	$n = 20$	$n = 5$	$n = 10$	$n = 20$
Circular solid disk	$\overline{w}$	0.3	-40.5469	35.1355	-15.0856	-3.3389	-21.0125	-19.5529
		0.5	-38.5304	33.1359	-15.1883	-4.1221	-20.7533	-19.7939
		0.7	-27.5894	22.6266	-15.0736	-6.2801	-18.4111	-20.2961
	$\overline{N}_r$	0.3	8.6779	11.1009	9.9916	8.5994	8.7328	9.0839
		0.5	6.1238	7.9906	7.2001	5.9749	6.1775	6.4451
		0.7	3.8832	4.0293	4.0819	3.3727	3.5563	3.5407
	$\overline{M}_r$	0.3	-5.3979	5.5183	0.3488	1.9789	-0.5607	0.6607
		0.5	-12.1289	11.1681	0.2222	3.5358	-1.7232	0.8247
		0.7	-2.8511	14.9594	-3.5389	-2.2204	-10.4352	-2.7318
		0.3	0.21138	0.21135	0.21135	0.22913	0.229083	0.229083

	$\overline{Q}_r \times 10^3$	0.5	1.646265	1.64288	1.642683	1.796728	1.792142	1.791889
		0.7	6.993439	6.929957	6.90587	7.684698	7.59787	7.566041
Mounted free hollow disk	$\overline{w}$	0.3	-0.1634	-0.4581	-0.7938	-0.1439	-0.2237	-0.2418
		0.5	-0.6454	-6.0402	-12.2359	0.0839	-1.1313	-1.2006
		0.7	-0.3597	-35.5466	-75.6892	4.6634	-2.7891	-2.9318
	$\overline{N}_r$	0.3	11.0613	16.1745	27.3155	9.7524	10.7592	10.7342
		0.5	7.0898	10.7947	19.8356	6.1834	6.8763	6.8459
		0.7	3.9989	4.8689	10.6742	3.5937	3.7225	3.6681
	$\overline{M}_r$	0.3	1.1161	15.6092	32.2686	-0.8299	2.0402	2.1388
		0.5	0.1195	30.1793	64.7427	-4.0628	1.6693	1.6994
		0.7	-2.1865	50.3772	115.1361	-2.3239	-3.6189	-2.9852
	$\overline{Q}_r \times 10^2$	0.3	-3.2093	-3.5208	-3.8105	-3.4484	-3.8187	-4.1607
		0.5	-2.5157	-2.7649	-3.0048	-2.7013	-2.9978	-3.2809
		0.7	-1.875	-2.0224	-2.2345	-2.0084	-2.1865	-2.4369
Mounted hollow supported cased disk	$\overline{w}$	0.3	-0.3111	2.9061	10.144	-0.5939	-0.3236	-0.5518
		0.5	-1.3197	9.2752	37.514	-2.0182	-1.5963	-2.6433
		0.7	-1.2728	7.4406	63.678	-1.3775	-4.1105	-7.0223
	$\overline{N}_r$	0.3	11.2376	12.2615	14.7917	10.2657	10.8699	11.0726
		0.5	7.2064	8.2306	11.6698	6.5187	6.9479	7.0635
		0.7	4.0598	3.8808	6.6358	3.7685	3.7583	3.7749
	$\overline{M}_r$	0.3	2.3199	-11.7113	-56.4237	2.6279	2.8047	4.5086
		0.5	1.1857	6.1826	-12.9622	-1.0141	2.3376	3.7657
		0.7	-1.7288	31.7798	55.4721	0.1281	-3.1028	-1.4048
	$\overline{Q}_r$	0.3	-0.0605	0.6113	2.0644	-0.1149	-0.0561	-0.0971
		0.5	-0.0487	0.5078	1.7114	-0.0938	-0.0448	-0.0787
		0.7	-0.0415	0.4782	1.5918	-0.0848	-0.0356	-0.0669

8. Conclusions

The bending response of a rotating viscous porous disk with exponential thickness gradient with mechanical and physical properties is presented and discussed in this study. Studying the components of bending in a porous disk using the first-order shear deformation theory (FSDT). The solution method was done by seeing the porous, viscous disk of variable thickness. Therefore, the solution method was based on using the semi-analytical solution method to get displacements of the porous disk of variable thickness, then using the correspondence principle and Illyushin's approximation method, considering the disk as porous and viscous. Numerical results were presented and the difference in results with changes in the inhomogeneity parameter and porosity coefficient was explained. Graphs illustrating the time factor in the status of the viscous porous disk were also presented. A comparison between porous disk and non-porous disk for three different statutes of boundary conditions on the disk is presented and discussed. From this study, we can summarize the basic results in some points:

- The principle of lower total energy is effective and important in deducing the relationships of bending components.
- A noticeable change in the value of the bending components by changing the inhomogeneity parameter and the porosity factor in the porous disk with exponential thickness.
- The porosity coefficient and inhomogeneity parameter had a clear effect on the numerical results of bending components in the status of the porous disk and the non-porous disk.
- The semi-analytical solution is an efficient way to obtain a solution to the heat equation and the displacement equations.
- The correspondence principle and Illyushin's approximation technique are important items to obtain the solution for a viscous porous disk.
- Obtaining a state of stability and equilibrium for the bending components in the viscous porous disk by changing the relaxation time parameter.
- By choosing appropriate values for the inhomogeneity parameter and porosity factor, we can obtain particular values for bending components in the porous disc and the non-porous disc.
- The numerical results demonstrated the importance of the study in modern engineering designs and advanced industrial applications in helping to design a viscous annular disk with graduated properties and variable thickness under the effect of many external factors and influences.

References

[1] D. Chen, J. Yang, S. Kitipornchai, Free and forced vibrations of shear deformable functionally graded porous beams, *International Journal of Mechanical Sciences,* Vol. 108-109, pp. 14-22, 2016/04/01/, 2016.

[2] R. Tantawy, A. M. Zenkour, Effect of Porosity and Hygrothermal Environment on FGP Hollow Spheres under Electromechanical Loads, *Journal of Applied and Computational Mechanics,* Vol. 8, No. 2, pp. 710-722, 2022.

[3] M. Saadatfar, M. Zarandi, M. Babaelahi, Effects of porosity, profile of thickness, and angular acceleration on the magneto-electro-elastic behavior of a porous FGMEE rotating disc placed in a constant magnetic field, *Proceedings of the Institution of Mechanical Engineers, Part C: Journal of Mechanical Engineering Science,* Vol. 235, No. 7, pp. 1241-1257, 2021.

[4] K. Gao, Y.-L. Lei, J. Yang, Dynamic characteristics of functionally graded porous beams with interval material properties, *Engineering Structures,* Vol. 197, 07/25, 2019.

[5] R. Tantawy, A. Zenkour, Effects of Porosity, Rotation, Thermomagnetic, and Thickness Variation on Functionally Graded Tapered Annular Disks, 2023.

[6] K. Gao, W. Gao, B. Wu, D. Wu, C. Song, Nonlinear primary resonance of functionally graded porous cylindrical shells using the method of multiple scales, *Thin-Walled Structures,* Vol. 125, pp. 281-293, 04/01, 2018.

[7] M. Sobhy, A. M. Zenkour, Wave propagation in magneto-porosity FG bi-layer nanoplates based on a novel quasi-3D refined plate theory, *Waves in Random and Complex Media,* Vol. 31, No. 5, pp. 921-941, 2021.

[8] R. Tantawy, A. M. Zenkour, Even and Uneven Porosities on Rotating Functionally Graded Variable-thickness Annular Disks with Magneto-electro-thermo-mechanical Loadings, *Journal of Applied and Computational Mechanics,* Vol. 9, No. 3, pp. 695-711, 2023.

[9] H. Wu, J. Yang, S. Kitipornchai, Mechanical Analysis of Functionally Graded Porous Structures: A Review, *International Journal of Structural Stability and Dynamics,* Vol. 20, No. 13, pp. 2041015, 2020.

[10] R. Tantawy, Magneto-Electric Influence on a Functionally Graded Porous Hollow Structure in Hygrothermal Environment, *Scientific Journal for Damietta Faculty of Science,* Vol. 12, pp. 183-200, 12/01, 2022.

[11] H. Norouzi, A. Alibeigloo, Three dimensional static analysis of viscoelastic FGM cylindrical panel using state space differential quadrature method, *European Journal of Mechanics - A/Solids,* Vol. 61, pp. 254-266, 2017/01/01/, 2017.

[12] M. Allam, R. Tantawy, A. Yousof, A. Zenkour, Elastic and Viscoelastic Stresses of Nonlinear Rotating Functionally Graded Solid and Annular Disks with Gradually Varying Thickness, *Archive of Mechanical Engineering,* Vol. 64, 12/20, 2017.

[13] E. V. Dave, W. G. Buttlar, G. H. Paulino, H. H. Hilton, Graded viscoelastic approach for modeling asphalt concrete pavements, in *Proceeding of,* American Institute of Physics, pp. 736-741.

[14] S.-E. Kim, N. D. Duc, V. H. Nam, N. Van Sy, Nonlinear vibration and dynamic buckling of eccentrically oblique stiffened FGM plates resting on elastic foundations in thermal environment, *Thin-Walled Structures,* Vol. 142, pp. 287-296, 2019/09/01/, 2019.

[15] Z. Q. Cheng, S. A. Meguid, Z. Zhong, Thermo-mechanical behavior of a viscoelastic FGMs coating containing an interface crack, *International Journal of Fracture,* Vol. 164, No. 1, pp. 15-29, 2010/07/01, 2010.

[16] J. G. Yu, F. E. Ratolojanahary, J. E. Lefebvre, Guided waves in functionally graded viscoelastic plates, *Composite Structures,* Vol. 93, No. 11, pp. 2671-2677, 2011/10/01/, 2011.

[17] M. N. M. Allam, R. Tantawy, Thermomagnetic viscoelastic responses in a functionally graded hollow structure, *Acta Mechanica Sinica,* Vol. 27, No. 4, pp. 567-577, 2011/08/01, 2011.

[18] A. M. Dehrouyeh-Semnani, M. Dehrouyeh, M. Torabi-Kafshgari, M. Nikkhah-Bahrami, An investigation into size-dependent vibration damping characteristics of functionally graded viscoelastically damped sandwich microbeams, *International Journal of Engineering Science,* Vol. 96, pp. 68-85, 2015/11/01/, 2015.

[19] J. Deng, Y. Liu, Z. Zhang, W. Liu, Stability analysis of multi-span viscoelastic functionally graded material pipes conveying fluid using a hybrid method, *European Journal of Mechanics - A/Solids,* Vol. 65, pp. 257-270, 2017/09/01/, 2017.

[20] A. H. Sofiyev, On the solution of the dynamic stability of heterogeneous orthotropic visco-elastic cylindrical shells, *Composite Structures,* Vol. 206, pp. 124-130, 2018/12/15/, 2018.

[21] Y. Q. Mao, Y. M. Fu, H. L. Dai, Creep buckling and post-buckling analysis of the laminated piezoelectric viscoelastic functionally graded plates, *European Journal of Mechanics - A/Solids,* Vol. 30, No. 4, pp. 547-558, 2011/07/01/, 2011.

[22] M. H. Jalaei, Ö. Civalek, On dynamic instability of magnetically embedded viscoelastic porous FG nanobeam, *International Journal of Engineering Science,* Vol. 143, pp. 14-32, 2019/10/01/, 2019.

[23] A. Ebrahimi-Mamaghani, A. Forooghi, H. Sarparast, A. Alibeigloo, M. Friswell, Vibration of Viscoelastic Axially Graded Beams with Simultaneous Axial and Spinning Motions under an Axial Load, *Applied Mathematical Modelling,* Vol. 90, 09/23, 2020.

[24] S. Coskun, J. Kim, H. Toutanji, Bending, Free Vibration, and Buckling Analysis of Functionally Graded Porous Micro-Plates Using a General Third-Order Plate Theory, *Journal of Composites Science,* Vol. 3, pp. 15, 02/01, 2019.

[25] A. A. Daikh, A. M. Zenkour, Free vibration and buckling of porous power-law and sigmoid functionally graded sandwich plates using a simple higher-order shear deformation theory, *Materials Research Express,* Vol. 6, No. 11, pp. 115707, 2019/10/11, 2019.

[26] A. M. Zenkour, A quasi-3D refined theory for functionally graded single-layered and sandwich plates with porosities, *Composite Structures,* Vol. 201, pp. 38-48, 2018/10/01/, 2018.

[27] A. M. Zenkour, Quasi-3D Refined Theory for Functionally Graded Porous Plates: Displacements and Stresses, *Physical Mesomechanics,* Vol. 23, No. 1, pp. 39-53, 2020/01/01, 2020.

[28] Q. Li, D. Wu, X. Chen, L. Liu, Y. Yu, W. Gao, Nonlinear vibration and dynamic buckling analyses of sandwich functionally graded porous plate with graphene platelet reinforcement resting on Winkler-Pasternak elastic foundation, *International Journal of Mechanical Sciences,* Vol. 148, 09/01, 2018.

[29] S. Sahmani, M. Aghdam, T. Rabczuk, Nonlocal strain gradient plate model for nonlinear large-amplitude vibrations of functionally graded porous micro/nano-plates reinforced with GPLs, *Composite Structures,* Vol. 198, 05/01, 2018.

[30] M. Slimane, A. Hadj Mostefa, Y. Beldjelili, M. Merazi, S. Boutaleb, H. Hellal, Analytical solution for statif bending analyses of functionally grades plates with porosities, *Frattura ed Integrità Strutturale,* Vol. 55, 01/01, 2021.

[31] A. Zenkour, M. Aljadani, Quasi-3D Refined Theory for Functionally Graded Porous Plates: Vibration Analysis, *Physical Mesomechanics,* Vol. 24, pp. 243-256, 03/01, 2021.

[32] A. Zenkour, M. Aljadani, Porosity effect on thermal buckling behavior of actuated functionally graded piezoelectric nanoplates, *European Journal of Mechanics - A/Solids*, Vol. 78, pp. 103835, 08/01, 2019.

[33] Y. Ootao, Y. Tanigawa, Transient piezothermoelastic analysis for a functionally graded thermopiezoelectric hollow sphere, *Composite Structures*, Vol. 81, No. 4, pp. 540-549, 2007/12/01/, 2007.

[34] A. Ghorbanpour Arani, R. Kolahchi, A. A. Mosallaie Barzoki, A. Loghman, Electro-thermo-mechanical behaviors of FGPM spheres using analytical method and ANSYS software, *Applied Mathematical Modelling*, Vol. 36, No. 1, pp. 139-157, 2012/01/01/, 2012.

[35] M. Allam, R. Tantawy, A. Zenkour, Thermoelastic stresses in functionally graded rotating annular disks with variable thickness, *Journal of Theoretical and Applied Mechanics (Poland)*, Vol. 56, pp. 1029-1041, 10/20, 2018.

[36] M. Bayat, M. Rahimi, M. Saleem, A. H. Mohazzab, I. Wudtke, H. Talebi, One-dimensional analysis for magneto-thermo-mechanical response in a functionally graded annular variable-thickness rotating disk, *Applied Mathematical Modelling*, Vol. 38, No. 19, pp. 4625-4639, 2014/10/01/, 2014.

[37] G. Paria, *Magneto-Elasticity and Magneto-Thermo-Elasticity*, in: G. G. Chernyi, P. Germain, L. Howarth, W. Olszak, W. Prager, R. F. Probstein, H. Ziegler, *Advances in Applied Mechanics*, Eds., pp. 73-112: Elsevier, 1966.

[38] M. Rouhi, A. Angoshtari, R. Naghdabadi, Thermoelastic analysis of thick-walled finite-length cylinders of functionally graded materials, *Journal of Thermal Stresses - J THERMAL STRESSES*, Vol. 28, pp. 391-408, 03/23, 2005.

[39] J. N. Reddy, C. M. Wang, S. Kitipornchai, Axisymmetric bending of functionally graded circular and annular plates, *European Journal of Mechanics - A/Solids*, Vol. 18, No. 2, pp. 185-199, 1999/03/01/, 1999.

[40] B. E. P. M.N.M. Allam, on the solution of quasi-statical problems of anisotropic viscoelasticity, *Isvestia Akademy Nauk, AR-SSR Mekhanika, ,* Vol. 31, pp. 19-27, 1976

[41] B. E. P. A.A. Illyushin, Foundation of mathematical theory of thermo viscoelasticity, *Nauka, Moscow*, 1970